CKB is regulated by thermogenic stimuli and is targeted to mitochondria by an internal matrix targeting signal-like sequence

Anna Roesler

Department of Biochemistry
McGill University, Montreal
December 2020

A thesis submitted to McGill University in partial fulfillment of requirements of the degree of Master's of Science

ABSTRACT

Brown and beige adipocytes exhibit immense capacity to increase energy expenditure by dissipating chemical energy as heat (thermogenesis) and can be leveraged to combat obesity in mice. The identification of functional thermogenic fat in adult humans has reinvigorated research into pathways controlling energy expenditure in these tissues. Uncoupling protein 1 (UCP1) plays a major role in thermogenesis, but it is now appreciated that multiple thermogenic pathways are also active in brown and beige adipocytes. A futile cycle of creatine phosphorylation and dephosphorylation has been identified as a novel thermogenic mechanism that is active in mitochondria of brown and beige adipocytes. Initial data indicate that creatine kinase, brain-type (CKB) is the most abundant creatine kinase isoenzyme in brown adipocytes from mice and that loss of *Ckb* results in reduced oxygen consumption in these same cells. In line with a role in thermogenesis, data herein show that CKB levels are upregulated in brown fat of cold-exposed mice and upon treatment with CL 316-234 (CL), a specific β3-adrenergic receptor agonist. Intriguingly, stimulation of β3-adrenoceptor signaling does not increase CKB levels to the same extent as cold, indicating that input outside of the β3-adrenergic receptor regulates sympathetic induction of CKB in BAT. Biochemical methods establish CKB as a mitochondrial protein, but stable import into the organelle and percentage of mitochondria-localized CKB is highly cell type-specific. Approximately 10% of the total CKB pool is localized to mitochondria in brown fat, a much higher proportion (~30 fold) compared to other tissues examined. Moreover, CKB harbours an internal matrix targeting signal-like (iMTS-L) sequence that is important for mitochondrial import as mutation of key iMTS-L residues hindered CKB internalization into mitochondria. Lastly, CKB-deficient brown adipocyte mitochondria do not exhibit futile creatine cycling unlike mitochondria from CKB-expressing cells. Overall, the results of this study indicate that CKB is targeted to mitochondria through an iMTS-L where it controls creatine cycling in brown fat.

RÉSUMÉ

Les adipocytes bruns et beiges présentent une immense capacité à augmenter la dépense énergétique en dissipant l'énergie chimique sous forme de chaleur (thermogénèse) et peuvent être mis à profit pour lutter contre l'obésité chez les souris. L'identification de la graisse thermogénique fonctionnelle chez l'homme adulte a redynamisé la recherche sur les voies de contrôle de la dépense énergétique dans ces tissus. La protéine de découplage 1 (UCP1) joue un rôle majeur dans la thermogénèse, mais on sait maintenant que plusiers voies thermogènes sont également actives dans les adipocytes bruns et beiges. Un cycle futile de phosphorylation et de déphosphorylation de la créatine a été identifié comme un nouveau mécanisme thermogénique actif dans les mitochondries des adipocytes bruns et beiges. Les premières données indiquent que la créatine kinase de type cérébral (CKB) est l'isoenzyme de créatine kinase la plus abondante dans les adipocytes bruns des souris et que la perte de *Ckb* peut provoquer une réduction de la consommation d'oxygène dans ces mêmes cellules. Conformément à un rôle dans la thermogenèse, les données présentées ici montrent que les niveaux de CKB sont régulés à la hausse dans la graisse brune des souris exposées au froid et lors du traitement avec la CL 316-234 (CL), un agoniste spécifique du récepteur 3-adrénergique. Il est intriguant de constater que la stimulation de la signalisation des 3-adrénorécepteurs n'augmente pas les niveaux de CKB dans la même mesure que le froid, ce qui indique qu'une entrée en dehors du récepteur 3-adrénergique régule l'induction sympathique de la CKB dans les MTD. Les méthodes biochimiques établissent que la CKB est une protéine mitochondriale, mais l'importation stable dans l'organite et le pourcentage de CKB localisée dans la mitochondrie est hautement spécifique au type de cellule. Environ 10 % du pool total de CKB est localisé dans les mitochondries de la graisse brune, une proportion beaucoup plus élevée (~30 fois) par rapport aux autres tissus examinés. De plus, le CKB abrite une signal interne de ciblage matrice (iMTS-L) qui est importante pour l'importation mitochondriale car la mutation des principaux résidus iMTS-L a empêché l'internalisation du CKB dans les mitochondries. Enfin, les mitochondries des adipocytes bruns déficients en CKB ne présentent pas de cycle de créatine futile, contrairement aux mitochondries des cellules exprimant le CKB. Dans

l'ensemble, les résultats de cette étude indiquent que le CKB est ciblé sur les mitochondries par le biais d'un iMTS-L où il contrôle le cycle de la créatine dans la graisse brune.

ACKNOWLEDGEMENTS

First and foremost, I would like to thank my supervisor, Dr. Lawrence Kazak, for the guidance, encouragement, and passing down of knowledge I received from him throughout my Master's degree. My lab mates: Janane Rahbani, Bozena Samborksa, Faiz Hussain, and Christien Dykstra, and Miranda Medeiros, were also critical to my success and sanity. I am also thankful to advice received from the members of my research advisory committee, Drs. Heidi McBride and Jason Young. I would also like to thank my first mentor, Dr. Scot Leary, for providing me the opportunity to work in his lab as an undergraduate, and in whose lab my love for the mitochondrion was ignited. Lastly, I would like to shoutout my parents who have supported me in every endeavour and without whom, I literally wouldn't be here.

TABLE OF CONTENTS

ABSTRACT ii

RÉSUMÉ iii

ACKNOWLEDGEMENTS v

TABLE OF CONTENTS vi

LIST OF ABBREVIATIONS viii

PUBLICATIONS ARISING FROM THIS THESIS x

CONTRIBUTION OF AUTHORS x

I. INTRODUCTION 11

1.0 Background on Obesity 13

1.1 Obesity Prevalence and Associated Diseases 13

1.2 Obesity Pathogenesis 13

1.3 Obesity Therapeutics 14

2.0 White Adipose Tissue 15

2.1 Energy Storage in WAT 15

2.2 Mechanism of WAT Expansion and Contraction 15

3.0 Brown Adipose Tissue 16

3.1 Introduction to BAT Thermogenesis 16

3.2 Identification of BAT in Adult Humans 17

3.3 Sympathetic Activation of BAT 18

3.4 Mitochondrial respiratory control 19

3.5 Thermogenesis through UCP1 20

3.6 Beige adipocytes 20

3.7 UCP1-Independent Thermogenesis 21

3.8 Phosphocreatine shuttle 22

3.9 Thermogenic Creatine Cycling 22

3.10 Physiological Relevance of Thermogenic Creatine Cycling 24

4.0 Mitochondrial Protein Import 24

4.1 Basics of Mitochondrial Protein Import 24

4.2 Presequence Import Pathway 25

4.3 Metabolite Carrier Import and Insertion into the Inner Membrane 26
4.4 Mia40-Dependent Import of Intermembrane Space Proteins 26
4.5 Sorting of Outer Mitochondrial Membrane Proteins 27
4.6 Mitochondrial Protein Import Conclusion 27

III. MATERIALS AND METHODS 28

IV. RESULTS 37

V. FIGURES 48

Figure 1. CKB is regulated by cold selectively in BAT 50
Figure 2. CKB levels are regulated by β3-adrenergic receptor signaling 52
Figure 3. Stimulation of α1-adrenoceptors increases CKB levels in primary brown adipocytes 53
Figure 4. CKB is localized to brown adipocyte mitochondria 55
Figure 5. The mitochondrial targeting sequence of CKB is not contained with the first 40 amino acids or within the CX_4C cysteine motif 57
Figure 6. CKB is targeted to mitochondria through an iMTS-L 58
Figure 7. CKB internalization into mitochondria is cell-type dependent 61

VI. DISCUSSION 62

VII. CONCLUSIONS 69

VIII. REFERENCES 71

LIST OF ABBREVIATIONS

^{18}F-FDG	^{18}F-2-fluoro-D-2-deoxy-D-glucose
ATP	adenosine triphosphate
BAT	brown adipose tissue
BCA	bicinchoninic assay
BMI	body mass index
BSA	bovine serum albumin
CKB	creatine kinase, brain-type
CKM	creatine kinase, muscle-type
CKMT1	creatine kinase ubiquitous-type, mitochondrial
CKMT2	creatine kinase sarcomeric-type, mitochondrial
CL	CL 316,243
CREB	cAMP response element binding-protein
DMSO	dimethyl sulfoxide
DNP	2,4-dinitrophenol
EDTA	ethylenediaminetetraacetic acid
ERK	extracellular signal-regulated kinase
ETC	electron transport chain
FBS	fetal bovine serum
FFA	free fatty acid
GATM	glycine amidinotransferase
GDP	guanine diphosphate
GPCR	G-protein coupled receptors
GTP	guanine triphosphate
HEPES	4-(2-hydroxyethyl)-1-piperazineethanesulfonic acid
HFD	high-fat diet
HSL	hormone-sensitive lipase
IBMX	isobutylmethylxanthine
IMS	intermembrane space
iMTS-L	internal matrix targeting signal-like

KRBMB	Krebs-Ringer Bicarbonate Modified Buffer
LD	lipid droplet
LPL	lipoprotein lipase
MEF	mouse embryonic fibroblast
MIM	mitochondrial import complex
MPP	mitochondrial processing peptidase
mTP	mitochondrial targeting prediction
N-MTS	N-terminal mitochondrial targeting sequence
NE	norepinephrine
NST	non-shivering thermogenesis
OXA	oxidase assembly translocase
PAM	presequence translocase-associated motor
PCr	phosphocreatine
PET-CT	positron-emission tomographic and computed tomographic
PGC-1α	peroxisome proliferator-activated receptor gamma coactivator-1α
P_i	inorganic phosphate
PKA	protein kinase A
PPARγ	peroxisome proliferator-activated receptor gamma
SAM	sorting and assembly machinery
SAT	subcutaneous adipose tissue
SVF	stromal vascular fraction
T3	triiodothyronine
TBS	tris-buffered saline
TBS-T	tris-buffered saline containing 0.005% Tween-20
TG	triglycerides
TIM23	translocase of the inner membrane
TOM	translocase of the outer membrane
UCP1	uncoupling protein 1
VAT	visceral adipose tissue
WAT	white adipose tissue

PUBLICATIONS ARISING FROM THIS THESIS

Rahbani, J.F., **Roesler, A.,** Hussain, M.F., Samborska, B., Jesperson, N.Z., Tsai, L., Dykstra, C.B., Jedrychowski, M.P., Vergnes, L., Reue, K., Scheele, C., Spiegelman, B.R., and Kazak, L. Creatine kinase B triggers futile creatine cycling in thermogenic fat. *Nature.* (Accepted for publication).

CONTRIBUTION OF AUTHORS

All work presented in this thesis were performed by me (AR) with the exception of the following: 1) All RT-qPCR analysis was done by Janane Rabhani (JR) on samples harvested by AR; 2) The CKB^{FLAG} mouse was generated by Faiz Hussain (FH); 3) Creatine kinase activity assays were performed by FH on samples prepared by AR. Figures were generated by AR and Dr. Lawrence Kazak.

I. INTRODUCTION

Rates of obesity are rapidly increasing worldwide, to the point where obesity is considered a global epidemic. It is well documented that obesity is often linked to an array of other diseases such as cardiovascular disease, type II diabetes, and cancer. Thermogenesis by brown and beige adipocytes has been shown to combat obesity and associated metabolic disease by increasing whole body energy expenditure. Uncoupling protein 1 (UCP1) has long been considered the main effector of adipocyte thermogenesis, but the last several years have seen the identification of new thermogenic pathways.

Futile creatine cycling is one recently uncovered mechanism that contributes to thermogenesis by promoting ATP turnover, leading to increased mitochondrial respiration. Creatine kinase enzymes catalyze the reversible phosphorylation of creatine using ATP as the phosphoryl group donor. There are four creatine kinase isoenzymes expressed in mammals which have been extensively studied in the context of the PCr shuttle, an energy buffering system that utilizes a mitochondrial form and a cytosolic form of creatine kinase. Typically, creatine kinase isoenzymes exhibit tissue-selective expression and subcellular localization. Being localized to the major site of ATP production, mitochondrial creatine kinases preferentially catalyze the forward creatine kinase reaction towards PCr generation. In “normal” creatine metabolism, the result of this reaction is liberation of ADP, which stimulates oxygen consumption in a manner that is directly proportional (1:1) to the amount of creatine consumed by the mitochondrial creatine kinase reaction. Previous studies have established that the addition of creatine to thermogenic fat cells leads to molar excess of ADP (compared to creatine consumed), that leads to excess oxygen consumption and drives thermogenic respiration.

Creatine cycling is hypothesized to result from two different enzymatic activities. First, a mitochondrial creatine kinase hydrolyzes ATP to phosphorylate creatine in a reaction that generates PCr and ADP. Second, it is thought that a phosphatase enzyme hydrolyzes PCr to regenerate creatine to be used for subsequent rounds of cycling. While the physiological significance of thermogenic creatine cycling has been demonstrated in

mice lacking adipocyte creatine, no protein has yet been shown to directly control the creatine cycle. Preliminary data from our laboratory indicates that CKB is the most abundant creatine kinase isoenzyme in brown adipocytes purified from mice and that loss of *Ckb* results in blunted rates of oxygen consumption in the same cell type.

CKB is generally described of as a cytosolic protein. Thus, because creatine cycling is thought to occur in mitochondria from brown adipocytes, we hypothesized that at least a fraction of CKB was partitioned to brown adipocyte mitochondria to control this cycle. Since CKB has never been studied in brown fat, the first aim of this research was to characterize the response of brown fat CKB to thermogenic stimuli, primarily through assessing CKB levels in response to cold exposure, a common method of inducing brown fat thermogenesis. The second aim of this study was to use biochemical methods to examine the presence of CKB in brown fat mitochondria and to determine the targeting signals that direct CKB to the organelle. Overall, this study sought to establish the thermogenic response of CKB in brown adipocytes and to determine the signals that govern mitochondrial localization of CKB.

II. LITERATURE REVIEW

1.0 Background on Obesity

1.1 Obesity Prevalence and Associated Diseases

The global prevalence of obesity and excess bodyweight has tripled over the last four decades and continues to increase at an alarming rate, becoming one of the greatest challenges to health in today's society[1]. The most common method for classifying overweight and obesity in adults is body mass index (BMI), a simple measure of body weight as a function of height. BMI is defined as an individual's mass (measured in kilograms, kg) by the square of their height (measured in meters, m) and a BMI greater than 30 kg/m^2 is classified as obese[2,3]. Though imperfect because muscle mass, body fat percentage, and sex are not accounted for, BMI remains a widely used and reliable measure of population-level overweight and obesity levels but not as an individual diagnostic tool[4-6]. In Canada, more than half of the population is estimated to be overweight or obese based on BMI[7].

Obesity is intricately linked with overall increased mortality[8,9] as well as an increased risk for developing an array of comorbidities including type 2 diabetes[10,11], cardiovascular disease[12,13], and certain types of cancer[14-16]. Thus, obesity is associated with major adverse health concerns and massive economic burden on the healthcare system and can only be overcome with effective prevention and treatment[17].

1.2 Obesity Pathogenesis

Obesity results when energy intake chronically exceeds energy expended by the body[18]. Prolonged positive energy balance results in increased lipid accumulation, primarily in adipose tissue, which leads to weight gain[19]. Energy intake is defined as calories consumed from food or drink, whereas energy expenditure has several major components: physical activity, obligatory energy expenditure (energy required to perform cellular functions and is also associated with digestion), and adaptive non-shivering thermogenesis (NST), defined as heat production independent of muscle activity (i.e.

shivering). Historically, obesity has been viewed as the result of negative traits including lack of willpower, gluttony and/or laziness. However, based on an ever-increasing body of literature, we now know that obesity pathogenesis is much more complex than just the overconsumption of calories and that some individuals are pre-disposed to weight gain[20-23]. It is difficult to pinpoint the exact etiology of obesity as it is a multifactorial disease that arises from interactions between various genetic, physiological, socio-behavioural, and environmental factors that ultimately result in a net positive energy balance over time[20-26]. Adding to the complexity of obesity pathogenesis, the combination of these interactions that lead to obesity vary on an individual basis and can change over time.

1.3 Obesity Therapeutics

Lifestyle intervention, in the form of increased physical activity and/or reduced caloric intake, is the foundation for combatting obesity[27,28]. However, as evidenced by the ever-increasing rate of population-level obesity, it is not a realistic strategy for combatting obesity as patient adherence is low and even for those who do initially lose weight, long-term maintenance of weight loss is often unsustainable[29]. Aside from lifestyle modification, surgical and pharmaceutical interventions are alternative/complementary approaches to weight loss. In North America, the only pharmaceuticals currently approved for treating obesity act to suppress energy intake by inhibiting intestinal fat absorption or by targeting neuronal hunger pathways to repress food intake. While these drugs can be effective, they have had limited success as individual responses vary widely and significant side effects have been reported, such as nausea and constipation[30]. An alternative approach to combatting obesity could be through activation of pathways controlling energy expenditure to increase metabolic rate and “burn” excess fat. Although obesity is associated with increased body fat content (and as a result adipose tissue is most often viewed in a negative light), functionally and developmentally distinct types of adipocytes exist in mammals, some even exhibiting anti-obesogenic effects[31].

2.0 White Adipose Tissue

2.1 Energy Storage in WAT

White adipose tissue (WAT) is the major reservoir for storing metabolic fuel/excess energy in mammals and can account for as little as 5% bodyweight and up to 50% bodyweight in humans[32]. Metabolic fuel is stored in the form of triglycerides (TGs) contained within cytoplasmic lipid droplets (LDs) of white adipocytes. Lipids serve as specialized energy storage molecules because they are efficiently stored in anhydrous form and offer more energy upon complete oxidation (~9 kilocalories/gram) compared to carbohydrate and protein (~4 kilocalories/gram). While most eukaryotic cells are capable of LD biosynthesis, the large storage capacity that white adipocytes accommodate would be highly toxic to other cell types. Morphologically, white adipocytes typically contain a single, large LD that occupies up to 90% of cell volume and is the main determinant of cell size. Adipose tissue expands by increasing cell size (hypertrophy) and/or the number of adipocytes (hyperplasia). WAT can be roughly divided into two types: subcutaneous adipose tissue (SAT) and visceral adipose tissue (VAT). SAT is situated in a layer sitting directly beneath the skin whereas VAT is found between organs of the abdominal cavity. Unlike SAT, visceral fat expansion is strongly associated with the negative metabolic complications that are associated with obesity. This is because unhealthy WAT expansion leads to adipose tissue inflammation, macrophage infiltration, and increased pro-inflammatory cytokine signaling that ultimately leads to systemic inflammation, insulin resistance, and even fibrosis[33-40].

2.2 Mechanism of WAT Expansion and Contraction

WAT is an extraordinarily dynamic tissue and its abundance is determined by the balance between lipid synthesis/uptake and breakdown. The primary purpose of WAT is to expand and store energy during times of energy surplus (i.e. caloric excess) and release stored energy during times of energy deprivation (i.e. fasting). In the fed state, excess circulating lipids from the diet are hydrolyzed by lipoprotein lipase (LPL) and released as free fatty acids (FFAs) for re-esterification into TGs for storage in adipose

tissue. Alternatively, fatty acids generated through *de novo* lipogenesis can also be esterified to TGs and contribute to adipocyte LD expansion. As glucose becomes limiting in the fasting state, stored TGs are rapidly hydrolyzed into FFAs and glycerol by hormone-sensitive lipase (HSL), both of which are readily mobilized to the bloodstream for systemic use. Glycerol is mainly transported to the liver where it is metabolized to the glycolytic/gluconeogenic intermediate, glyceraldehyde 3-phosphate, whereas FFAs are transported to tissues with high energy demand, such as skeletal muscle and the heart. Once taken up by peripheral tissues, FFAs undergo beta-oxidation to generate acetyl-CoA, a precursor of adenosine triphosphate (ATP) synthesis. ATP is the main energy currency of the cell. Beyond the function of storing energy, WAT is also regarded as an endocrine organ that plays a major role in whole body energy homeostasis[41]. WAT secretes many hormones, cytokines, and peptides (collectively known as "adipokines") such as leptin, adipsin, and resistin that are released in response to different nutritional cues and regulate energy metabolism[42,43].

3.0 Brown Adipose Tissue

3.1 Introduction to BAT Thermogenesis

Brown adipose tissue (BAT) is developmentally and functionally distinct from WAT and is an organ unique to placental (eutherian) mammals[44]. Brown adipocytes encompass the major cell type and the functional unit of BAT that are specialized for energy dissipation and heat production through NST. Independent from heat production through muscle shivering, NST is also an important regulator of thermal homeostasis and was first described as an important mechanism for the survival of newborn mammals in the cold environment following birth, as well as for the arousal of hibernating animals during torpor[45,46]. Though BAT was first identified in hibernating marmots nearly 500 years ago[47], the quantitative contribution of BAT to thermogenesis was unclear until the late 1970's when studies using radiolabeled microspheres to map tissue blood flow demonstrated that brown fat could account for up to 60% of heat output in cold-acclimated rats[48,49].

It wasn't until 1979 when a seminal study by Rothwell and Stock showed that BAT thermogenesis is activated to a similar extent during cold exposure and following high-calorie feeding ("cafeteria diet") in rats[31]. The increase in energy expenditure that follows high-calorie feeding is referred to as "diet-induced thermogenesis" and appeared to play a protective role in bodyweight regulation, as cafeteria-fed rats exhibit a lower metabolic efficiency (gram weight gained per kcal eaten) compared to control-fed animals[31]. These observations laid the foundation of BAT as an anti-obesogenic tissue with a fundamental role in energy balance. In support of this, it has since been demonstrated several animal models exhibiting defective BAT thermogenesis are susceptible to diet-induced obesity[50,51].

3.2 Identification of BAT in Adult Humans

It was once thought that brown fat largely regressed in humans shortly following birth. However, in the late 2000's, studies using ^{18}F-2-fluoro-D-2-deoxy-D-glucose (^{18}F-FDG) combined with positron-emission tomographic and computed tomographic (PET-CT) scanning unequivocally revealed that adult humans possess significant depots of brown fat. Similar to rodents, it has been demonstrated that human brown fat is activated upon cold-exposure[52-58] and following carbohydrate-rich meals[59,60]. The major BAT depot of adult humans is located in the supraclavicular and neck regions although great variation exists within the population with respect to BAT abundance and metabolic activity. Numerous studies have found that the BAT mass is inversely correlated with BMI and other metabolic health parameters including waist circumference and waist-to-hip ratio[52,61-64]. Moreover, activation of human brown fat has been shown to improve insulin sensitivity and increase glucose uptake, improving whole-body glucose homeostasis as a result[65]. These observations support a role for BAT in regulating whole-body energy metabolism in humans and in the midst of the global obesity epidemic, has reinvigorated research into BAT as a viable anti-obesity target and a tissue that can uncouple obesity from disease.

3.3 Sympathetic Activation of BAT

BAT is dispersed in discrete regions throughout the body and can vary between species. In many mammals, including mice and newborn humans, the major BAT depot is located in the interscapular region where it receives dense innervation by sympathetic nerves and is highly vascularized to support efficient heat distribution to the rest of the body[66,67]. Unlike white adipocytes, brown adipocytes tend to contain small, multilocular LDs and are abundant in mitochondria that exhibit high metabolic activity upon sympathetic stimulation. Norepinephrine (NE) released from sympathetic neurons (such as during cold exposure and following high calorie feeding) is the most physiological relevant and potent stimulus that activates BAT[68,69]. NE exerts its effects through adrenergic receptors, a class of G-protein coupled receptors (GPCRs) that are expressed on the surface of the cell and mediate catecholamine-induced intracellular signaling cascades. There are two classes of adrenergic receptors: α- and β-adrenergic receptors that can further be separated into subclasses that exhibit varying affinities and responses towards NE and other catecholamines[70].

Expression of the β3-adrenergic receptor is restricted to adipocytes and is thought to be the principal mediator of NE-induced thermogenic signaling in brown fat in rodents[71]. Activation of the β3-adrenergic receptor leads to elevated cAMP levels and stimulates lipolysis through activation of protein kinase A (PKA), which phosphorylates and activates HSL, a key lipolytic enzyme. Lipolysis releases intracellular FFAs which serve to provide reducing equivalents (NADH, $FADH_2$) to the electron transport chain (ETC) and support the enhanced respiratory capacity of BAT that follows sympathetic stimulation. Moreover, PKA activates the transcription factor, cAMP response element binding-protein (CREB)[72,73], which in turn promotes expression of a thermogenic gene program in brown adipocytes. Among CREB targets is peroxisome proliferator-activated receptor gamma (PPARγ) coactivator-1α (PGC-1α)[74], which is often regarded as the master regulator of mitochondrial biogenesis and plays a key role in adaptive thermogenesis[75-77]. Most importantly, sympathetic stimulation allows brown adipocytes to bypass the constraints of mitochondrial respiratory control that normally govern substrate oxidation and ATP synthesis, a phenomenon unique to the thermogenic adipocytes.

3.4 Mitochondrial respiratory control

Mitochondria are responsible for generating most of the energy, in the form of ATP, needed by the cell through oxidative phosphorylation. Oxidative phosphorylation is the combination of two closely connected components: chemiosmosis and electron transport through the ETC, dual processes that are tightly coupled in most cell types. The ETC is comprised of a collection of protein complexes, termed complexes I-IV, and organic molecules that reside in the inner mitochondrial membrane of most eukaryotic cells. Mitochondrial respiration is initiated when reducing equivalents (NADH and $FADH_2$) donate electrons to either complex I (electrons from NADH) or complex II (electrons from $FADH_2$) of the ETC and simultaneously regenerate NAD^+ and FAD to be used in earlier steps of cellular metabolism (i.e. glycolysis, pyruvate oxidation, citric acid cycle). Through a series of oxidation-reduction reactions, electrons move from a higher to lower energy state as they are passed between the complexes of the ETC before ultimately reaching the final electron acceptor, molecular oxygen (O_2). Energy is released from electrons moving “downhill” in the energy gradient, and this energy is exploited by ETC complexes I, III, and IV to pump protons (H^+) across the inner mitochondrial membrane and into the intermembrane space (IMS), establishing an electrochemical proton gradient across the inner membrane. Since the inner mitochondrial membrane is impermeable to many ions, including H^+, protons can only return to the matrix by way of a transporter or channel. In most cells, ATP synthase (sometimes referred to as complex V of the ETC), harnesses the energy stored in the electrochemical gradient to move protons from the IMS to the matrix while concomitantly generating ATP.

ATP synthase is composed of two main subunits: F_1 and F_o. The F_1 subunit protrudes into the mitochondrial matrix and is a molecular motor responsible for ATP synthesis while the F_o is a proton pore embedded in the inner mitochondrial membrane. Proton flow through F_o drives rotation of the c ring of the F_1 subunit, inducing conformational changes that enable synthesis of ATP from ADP and inorganic phosphate (P_i). Chemical agents such as the proton ionophore 2,4-dinitrophenol (DNP), can uncouple electron transport from ATP synthesis by shuttling protons across biological membranes, thereby increasing substrate flux through the ETC (to maintain membrane

potential across the inner mitochondrial membrane) in the absence of increased ATP synthesis. Uncoupling proteins, of which there are five known homologs in mammals, provide a biological mechanism of separating substrate oxidation from ATP synthesis. Although only one, uncoupling protein 1 (UCP1) has been demonstrated to uncouple respiration from ATP synthesis *in vivo*[78,79].

3.5 Thermogenesis through UCP1

The best characterized mechanism by which brown adipocytes generate heat is through the action of UCP1, a protein that is selectively expressed in brown adipocytes and resides in the inner mitochondrial membrane[80]. UCP1 is a H^+/fatty acid symporter[81] whose primary function is to dissipate the electrochemical gradient across the inner mitochondrial membrane by providing an alternate route for protons to re-enter the matrix that is independent of ATP synthase[82-84]. By providing an alternative means for protons to enter the matrix, UCP1 frees brown fat mitochondria from the restraints of respiratory control that normally dictate and control the rate of substrate oxidation. As mitochondria strive to maintain membrane potential, the result of UCP1 activation is to greatly increase substrate flux through the ETC without increased ATP production (i.e. uncoupling), resulting in heat production as a byproduct of the oxidative reactions fueling mitochondrial respiration.

Under normal (ie: unstimulated) conditions, proton conductance through UCP1 is inhibited by physiological concentrations of purine nucleotides like ADP, ATP, guanine diphosphate (GDP), and guanine triphosphate (GTP), which directly bind UCP1 and prevent proton leak through this transporter[82,85]. Upon sympathetic stimulation of adrenergic receptors, FFAs liberated through lipolysis are direct allosteric activators of UCP1 and once bound, are sufficient to overcome the inhibition of UCP1 by purine nucleotides, although the exact mechanism remains controversial[86].

3.6 Beige adipocytes

It is now appreciated that brown fat-like cells, termed “beige” or “brite (brown in white)” adipocytes, are a distinct subset of adipocytes found interspersed within WAT of

rodents and humans[87]. Under basal conditions, beige adipocytes morphologically and functionally resemble white adipocytes. Upon activation with various agents including cold and administration of selective β3-adrenergic receptor agonists, beige adipocytes acquire a more "brown" phenotype including high UCP1 levels and activity, increased mitochondrial biogenesis, and enhanced ability to respond to sympathetic stimuli as evidenced by increased respiration rates and energy expenditure[88,89].

3.7 UCP1-Independent Thermogenesis

While UCP1 is no doubt important for thermogenesis in brown fat, several lines of evidence suggest that thermogenic mechanisms distinct from UCP1 are functional in both brown and beige fat, at least in rodents. First, mice lacking UCP1 are still able to maintain their core body temperature, without an increase in magnitude or frequency of muscle shivering[90]. However, cold tolerance in the absence of UCP1 seems to be dependent on mouse strain as UCP1-KO F1 hybrid mice generated from crossing C57BL/6J and 129/Sv1mJ animals are able to maintain body temperature when exposed to cold, whereas mice bred on either congenic background lose body temperature rapidly upon cold exposure[90,91]. Furthermore, congenic strains of UCP1-KO mice are able to defend their core body temperature when gradually acclimated to 4°C[92]. Thus, that some UCP1-KO mice can defend their body temperature suggests alternative thermogenic pathways are active in these mice. Second, mice with brown fat ablation (~95%) develop severe obesity on a chow diet[93], whereas UCP1-KO mice are protected from weight gain even when challenged with a high-fat diet (HFD)[94]. Based on the propensity of mice to gain weight following loss of brown fat, but not UCP1, suggests that a thermogenic pathway(s) is lost in brown-fat ablated mice that is still present in UCP1-KO mice.

The past five years have seen the identification of UCP1-independent thermogenic mechanisms and the field is currently in the middle of defining the molecular and regulatory characteristics of these pathways[95,96]. One such mechanism has been proposed to act through a cycle of futile creatine phosphorylation/dephosphorylation in the mitochondria of brown and beige adipocytes[96]. This is distinct from the currently

understood and defined pathway of creatine utilization, that is as a central metabolite of the phosphocreatine (PCr) shuttle.

3.8 Phosphocreatine shuttle

The PCr shuttle acts as an energy buffering system to move ATP equivalents from its site of production in the mitochondria to other cellular sites where it is needed to produce work[97]. This is a particularly important mechanism in myofibrils during muscle contraction[98]. The PCr shuttle relies on the activity of creatine kinases, enzymes that catalyze the reversible phosphoryl transfer from ATP to creatine[99]. When a cell is in a metabolically active state, ATP accumulates in mitochondria, the major site of ATP production, where PCr levels are low. The disequilibrium between these two molecules favors the consumption of ATP and creatine, generating PCr and ADP through an enzymatic reaction catalyzed by a mitochondrial CK. PCr is a high-energy compound that can diffuse from the mitochondria into the cytosol, a feature distinct from ATP, another high-energy molecule. When ADP become levels become high signaling a need for energy, cytosolic CK operated in reverse and uses PCr to regenerate the ATP pool. These dual processes make up the PCr shuttle, and thus utilizes a mitochondrial CK along with a cytosolic form. There are four CK isoenzymes, each encoded by a distinct gene: creatine kinase ubiquitous-type, mitochondrial (CKMT1), creatine kinase sarcomeric-type, mitochondrial (CKMT2), creatine kinase, brain-type (CKB), and creatine kinase, muscle-type (CKM)[100,101]. Typically, expression of a single cytosolic CK and a single mitochondrial CK dominate in certain cell types[99]. For example, myofibrils usually express CKM and CKMT2 in combination, whereas CKB and CKMT1 are normally expressed together in the brain[99,101]. However, CK expression and function has rarely been studied outside the context of skeletal muscle, heart, or brain tissue and patterns could differ between cell types.

3.9 Thermogenic Creatine Cycling

The mitochondrial creatine kinase reaction liberates ADP which stimulates oxygen consumption (respiration). Based on the PCr shuttle, the amount of ADP liberation should

be directly proportional to the amount of creatine consumed since creatine and ATP exhibit a strict 1:1 stoichiometric relationship with PCr and ADP. However, a creatine-driven thermogenic pathway was first postulated in 2015 and was shown to stimulate respiration by releasing a molar excess of ADP (with respect to creatine) in thermogenic adipocytes[96]. Mechanistically, similar to the PCr shuttle, the thermogenic creatine cycle is proposed to utilize a mitochondrial creatine kinase to catalyze the conversion of creatine and ATP and subsequent generation of PCr and ADP within the mitochondria. As mentioned, ADP activates respiration whereas PCr is immediately hydrolyzed, leading to the release of creatine. Creatine is recycled to undergo continuous rounds of ADP liberation and futile phosphorylation/dephosphorylation, resulting in a surplus of oxygen consumption relative to what would be expected if ADP and creatine were metabolized in a 1:1 stoichiometric ratio[96].

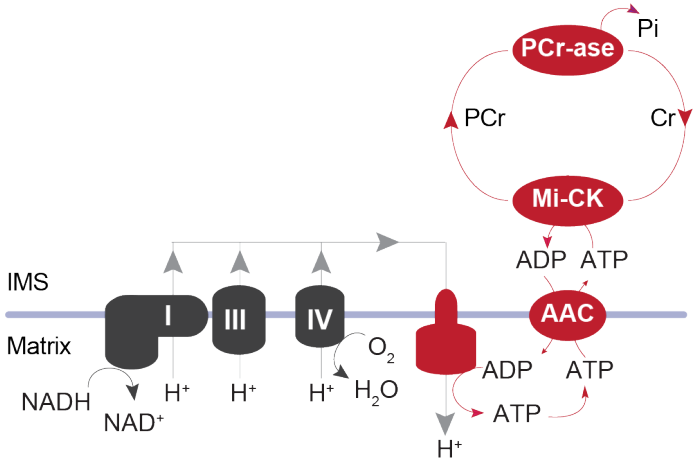

Figure 1: Thermogenic creatine cycling in mitochondria Creatine dissipates the energy stored in the protonmotive force by stimulating a cycle of ATP turnover, mediated by mitochondrial Creatine Kinase (Mi-CK) and coupled to the turnover of phosphocreatine (PCr). Mitochondrial ATP is used to drive the synthesis of PCr. This figure was originally published in Roesler & Kazak, *Biochem J* (2020)[102]

3.10 Physiological Relevance of Thermogenic Creatine Cycling

Adipocyte-specific deletion of the rate-limiting enzyme of creatine biosynthesis, glycine amidinotransferase (GATM) or the creatine transporter SLC6A8 leads to depletion of adipocyte creatine levels[103,104]. Both models have been used to study to physiological significance of thermogenic creatine cycling in mice and both exhibit blunted O_2 consumption in response to β3-adrenergic stimulation and gain more weight on a HFD compared litter-mate control animals[103,104]. Moreover, unlike wild-type animals, HFD feeding is unable to elicit increased metabolic rate in mice lacking GATM or SLC6A8[103,104], indicating a key role for creatine energetics in diet-induced thermogenesis and may largely explain the obese phenotype of these mice. Importantly, these effects of creatine depletion on NST are observed even in the presence of functional UCP1, providing further evidence that multiple thermogenic pathways are active and physiologically relevant in brown fat, at least in mice.

4.0 Mitochondrial Protein Import

4.1 Basics of Mitochondrial Protein Import

Mitochondria and the proteins that reside within the organelle are central to brown adipocyte function. Approximately 1300 proteins are found within mammalian mitochondria[105] and despite carrying its own genetic code and protein synthesis machinery, all but 13 proteins that reside within mitochondria are encoded by the nuclear genome and synthesized on cytosolic ribosomes[106,107]. Thus, most mitochondrial proteins must be post-translationally imported into the organelle[108]. Five mitochondrial import pathways have so far been identified and each depend on distinct signals in mitochondrial precursor proteins for directional import to the correct mitochondrial compartment. Mitochondria are double-membrane enclosed organelles. and contain four different sub-compartments: the outer and inner mitochondrial membranes which surround the IMS, and the area enclosed by the inner membrane termed the mitochondrial matrix. The translocase of the outer membrane (TOM) complex serves as the main import hub for most translocation pathways and consists of three outer membrane receptors: TOM20,

TOM22, and TOM70, the major channel-forming protein that polypeptides are transported through: TOM40, as well as three small Tom proteins (Tom6, Tom7, Tom8) that are important for the assembly and stability of the TOM complex[109-111].

4.2 Presequence Import Pathway

The best-defined pathway of mitochondrial protein import is termed the presequence pathway and protein import through this pathway is mediated through an N-terminal mitochondrial targeting sequence (N-MTS), also known as a presequence. Presequences are typically 15-50 amino acid residues in length and characteristically form amphipathic α-helices that are abundant in positively charged amino residues and are important for interacting with the import receptor TOM20[112-114]. The majority of proteins localized to the mitochondrial matrix and inner membrane contain a presequence and are imported into the organelle following recognition by both TOM20 and TOM22[115,116]. Once translocated across the outer mitochondrial membrane, presequence-containing preproteins are transferred to the translocase of the inner membrane (TIM23)[117,118]. The TIM23 complex is composed of various subunits that sort and direct preproteins towards the matrix, or if the preprotein contains a hydrophobic sorting signal, for lateral release into the lipid bilayer of the inner mitochondrial membrane[119]. Preprotein import through TIM23 is driven by membrane potential ($\Delta\psi$)[120,121], but full import and release into the matrix requires the activity of presequence translocase-associated motor (PAM) and its core subunit, mitochondrial Hsp70, an ATP-driven molecular chaperone[122-125]. Once in the matrix, presequences are typically cleaved and removed by mitochondrial processing peptidase (MPP) to reveal the mature protein[125].

Instead of being laterally released into the inner membrane, some inner membrane proteins are first imported into the matrix and then subsequently exported to the inner membrane by the oxidase assembly (OXA) translocase[126]. This pathway of inner membrane protein import is referred to as conservative sorting and is mediated by the main component of the OXA translocase, OXA1[127,128]. Until recently it was thought that OXA1-mediated insertion of inner membrane proteins was used only by a small number

of mitochondrial DNA-encoded proteins[126]. However, recent analysis of OXA1-deficient mitochondria revealed that numerous nuclear-encoded proteins depend on the OXA1 and the OXA translocase for inner membrane insertion and that OXA1 is essential to establish a functional inner mitochondrial membrane[129].

4.3 Metabolite Carrier Import and Insertion into the Inner Membrane

A separate family of inner membrane proteins are the metabolite carriers, which are synthesized in the cytosol and do not contain presequences situated in their N-termini. Instead, carrier proteins contain internal targeting sequences that have recently been shown to exhibit presequence properties but are instead situated downstream of the N-terminus[130]. These sequences, termed internal mitochondrial targeting sequence-like (iMTS-L), have been shown to be important for recognition and subsequent import by TOM70[131].

4.4 Mia40-Dependent Import of Intermembrane Space Proteins

Proteins destined for the mitochondrial IMS typically contain characteristic cysteine motifs. These motifs are commonly made up of two pairs of cysteine residues spaced three or nine amino acids apart and are referred to as twin CX_3C or CX_9C motifs, respectively. Import of cysteine-containing IMS proteins relies on a mitochondrial disulfide relay system, also known as the MIA pathway, that is mediated by two essential proteins, Mia40 and Erv1, and is also linked to the respiratory chain[132,133]. Mia40 is an oxidoreductase that promotes precursor translocation across the outer mitochondrial membrane and directly interacts with cysteine residues to catalyze the formation of disulfide bonds in incoming IMS precursors, promoting protein folding and stability[133-136]. Erv1 is a sulfhydryl oxidase[137] that keeps Mia40 in an oxidized state, thereby conferring Mia40 the ability to transfer disulfide bonds to incoming target proteins[133,138].

4.5 Sorting of Outer Mitochondrial Membrane Proteins

Two types of proteins are present in the outer mitochondrial membrane: β-barrel proteins containing several transmembrane segments, and α-helical proteins which are anchored to the outer membrane through at least one α-helical transmembrane segment. Precursor β-barrel proteins are synthesized in the cytosol and contain a hydrophobic β-hairpin element that directs these precursors to the TOM complex for mitochondrial translocation[139]. Once through the TOM channel and inside the IMS, small TIM chaperones bind to β-barrel precursors to prevent protein aggregation before outer membrane insertion by the sorting and assembly machinery (SAM) complex[140-142]. There are three main classes of α-helical outer membrane proteins: signal-anchored proteins, tail-anchor proteins, and polytopic (multi-spanning) proteins. α-Helical transmembrane segments are present in the N-terminus or C-terminus of signal-anchored and tail-anchored proteins, respectively. Along with serving as an outer membrane anchor signal, these transmembrane segments are also important for protein targeting and mitochondria recognition[143]. Conversely, the sequence(s) responsible for targeting polytopic α-helical proteins to the outer membrane have not yet been identified. The mitochondrial import (MIM) complex functions as a protein insertase for outer membrane insertion of both signal-anchored and polytopic α-helical proteins[144-146]. While Tom70 interacts with MIM to promote protein insertion, at least for polytopic α-helical proteins, the precise molecular mechanism of MIM-mediated insertion is presently unknown. In the case of tail-anchored proteins, no protein assembly and/or insertion machinery have been identified and the current evidence suggests that these proteins, as well as some polytopic proteins, are inserted in the outer membrane in a lipid-dependent manner[147-149].

4.6 Mitochondrial Protein Import Conclusion

Given the importance of mitochondria in cellular metabolism, protein import is tightly regulated and also functions as a sensor of mitochondrial fitness[150]. While much effort has gone into identifying the mechanisms governing mitochondrial protein import, much still remains to be discovered.

III. MATERIALS AND METHODS

Isolation of primary preadipocytes from murine brown adipose tissue

Interscapular BAT was dissected from 2-14 day old mice, washed in PBS, minced, and then digested for 45 minutes at 37°C with continuous shaking in buffer containing 1.5 mg/mL collagenase B (Roche), 123 mM NaCl, 5 mM KCl, 1.3 mM $CaCl_2$, 5 mM glucose, 100 mM 4-(2-hydroxyethyl)-1-piperazineethanesulfonic acid (HEPES), and 4% essentially fatty acid-free bovine serum albumin (BSA). The resulting tissue suspension was neutralized with adipocyte culture medium (DMEM/F12 with GlutaMAX (1:1, Invitrogen), 10% fetal bovine serum (FBS) and 1% PenStrep), filtered through a 100 μm cell strainer and centrifuged at 600 g for 5 min to pellet the stromal vascular fraction (SVF). The cell pellet was resuspended in adipocyte culture medium, filtered through a 40 μm cell strainer and centrifuged at 600 g for 5 min. The final pellet was resuspended in adipocyte culture medium and plated onto polystyrene cell culture dishes (Corning). SVF from five mice were plated onto a single 10-cm plate. Preadipocytes attach to the bottom of the dish whereas other cell types remain in suspension and were washed off the next day. A single plate containing preadipocytes was passaged twice up to ten, 10-cm dishes. Cells from each dish were frozen in freezing media (90% FBS, 10% dimethyl sulfoxide (DMSO)) and stored in liquid nitrogen at ~70-80% confluency. For mitochondrial preparations, cells were kept fresh and grown to post-confluency and differentiated into brown adipocytes.

In vitro brown adipocyte differentiation

Preadipocytes (from fresh or frozen stocks) were grown to post-confluency and differentiation was induced by treating cells with an adipogenic cocktail containing 1 μM rosiglitazone, 0.5 mM isobutylmethylxanthine (IBMX), 5 μM dexamethasone, 0.114 μg/mL insulin, 1 nM triiodothyronine (T3), and 125 μM indomethacin. Cell culture medium was replaced every 48 hours and was supplemented with an adipogenic maintenance cocktail

containing 1 μM rosiglitazone, 0.5 μg/mL insulin, and 1 nM T3. Cells were fully differentiated and used for experiments six days post-differentiation.

Mitochondria isolation from cultured brown adipocytes

To isolate mitochondria, two 15-cm dishes of differentiated brown adipocytes were gently scraped in 6 mL of hypotonic buffer (20 mM HEPES pH 7.8, 5 mM KCl, and 1.5 mM $MgCl_2$). Cells were homogenized on ice using 25 strokes of a tight-fitting Dounce homogenizer and quickly neutralized to a 1X MSH buffer (210 mM mannitol, 70 mM sucrose, 20 mM HEPES pH 7.8, and 5 mM ethylenediaminetetraacetic acid (EDTA)) using a 2.5X MSH stock. Homogenates were centrifuged at 8,500 g for 10 min at 4°C and the resulting fat layer was discarded. The pellet was resuspended in MSH buffer and centrifuged at 600 x g for 5 minutes at 4°C to pellet cellular debris and nuclei. Finally, the supernatant was spun at 8,500 x g for 10 minutes at 4°C to pellet mitochondria. Mitochondria were resuspended in an appropriate volume of MSH buffer (~20-40 μg/μL) and mitochondrial protein was quantified using the bicinchoninic assay (BCA) protein assay kit from Pierce.

Mitochondria isolation from murine tissue

Mice were sacrificed by cervical dislocation and tissue from 10 mice were harvested and pooled for one mitochondrial preparation. All steps were performed at 4°C. Dissected tissues were placed in SHE buffer (250 mM sucrose, 5 mM HEPES, 1 mM EGTA, 5% fatty acid-free BSA; pH 7.4) and then minced for 1-2 minutes on overturned beakers over ice. Minced tissue was homogenized in SHE buffer using ~10 strokes of a Teflon Pestle on medium speed. The resulting homogenate was filtered through two layers of cheesecloth and centrifuged at 8,500 x g for 10 minutes at 4°C. The resulting cell pellet was resuspended in SHE buffer and spun at 600 x g for 5 minutes at 4°C to pellet cellular debris and nuclei. Finally, the supernatant was spun at 8,500 x g for 10 minutes at 4°C to pellet mitochondria. Mitochondria were resuspended in an appropriate volume of

mitochondria storage buffer (100 mM KCl, 20 mM K-TES; pH 7.2) (~20-40 μg/μL) and mitochondrial protein was quantified using the BCA protein assay kit from Pierce.

Mitochondrial protease protection assays

For mitochondrial protease protection assays, 400 μg of mitochondrial protein was treated with 5 μg of trypsin in MSH buffer in a final reaction volume of 200 μL. Samples were incubated for 20 minutes at room temperature, rotating end over end. At the end of the assay, FBS was added to a final concentration of ~10% in each reaction to inhibit trypsin. Mitochondria were spun at 10,000 x g for 2 minutes at 4°C. The mitochondrial pellet was washed twice with PBS by rotating the tube and spinning at 10,000 g to pellet mitochondria to the other side of the tube. Lastly, mitochondria were lysed in adipocyte lysis buffer (50 mM Tris pH 7.4, 500 mM NaCl, 1% NP-40, 20% glycerol, 5 mM EDTA) supplemented with a protease inhibitor cocktail (Roche).

Purification of mature brown adipocytes by floatation technique

Interscapular brown fat was dissected from mice, washed in PBS, minced, and then digested for 45 minutes at 37°C with continuous shaking in Krebs-Ringer Bicarbonate Modified Buffer (KRBMB; 135 mM NaCl, 5 mM KCl, 1 mM $CaCl_2$, 1 mM $MgCl_2$, 0.4 mM K_2HPO_4, 25 mM $NaHCO_3$, 20 mM HEPES, 10 mM glucose, 4% fatty acid-free BSA), supplemented with 2 mg/mL collagenase B (Worthington) and 1 mg/mL soybean trypsin inhibitor (Worthington). Following digestion, the resulting tissue suspension was filtered through a 100 μM cell strainer and spun at 30 g for 5 minutes at room temperature. The infranatant was discarded and the floated adipocytes were washed twice with 20 mL KRBMB and again spun at 30 g for 5 minutes at room temperature. In between each wash, adipocytes were left to sit for 30 minutes at room temperature to allow adipocytes to float. Following the final spin, the infranatant was discarded and the mature, floated adipocytes were lysed in adipocyte lysis buffer and protein was quantified using the BCA protein assay kit from Pierce.

Gene Expression Analysis (RT-qPCR)

Total RNA was extracted from flash-frozen tissue using TRIzol reagent (Invitrogen). RNA was purified using RNeasy Mini spin columns (Qiagen) and reverse transcribed using a High-Capacity cDNA Reverse Transcription kit (Applied Biosystems). Resulting cDNA was analyzed by RT-qPCR. Briefly, 20 ng cDNA and 150 nmol of each gene primer were mixed with GoTaq qPCR Master Mix (Promega). Reactions were performed in a 384-well format using a CFX384 Real-time PCR system (Bio-rad). Normalized mRNA expression was calculated using the ΔΔCt method, using *Ppib* mRNA as the reference gene. The primer sequences used are listed in the following table:

RT-qPCR primers		
Gene name	**Fwd Sequence**	**Rev Sequence**
Ckb	GCCTCACTCAGATCGAAACTC	GGCATGTGAGGATGTAGCCC
Ckm	CCTCTATATAACCCAGGGGCACA	AGTGTCTGTCTGTGCTGTGGA
Ckmt1	TGAGGAGACCTATGAGGTATTTGC	TCATCAAAGTAGCCAGAACGGA
Ckmt2	CCAGTGCCTTCTCAAAGTTGC	AGTCCGCACTTGGGGGAAAGAG
Fabp4	AAGGTGAAGAGCATCATAACCCT	TCACGCCTTTCATAACACATTCC
Gamt	GCAGCCACATAAGGTTGTTCC	CTCTTCAGACAGCGGGTACG
Gatm	ATGCCTGTGTGCCACCATTC	TTGCACATCTCTTCGACCTCA
Pparg2	TGCCTATGAGCACTTCACAAGAAAT	CGAAGTTGGTGGGCCAGAA
Ppib	GGAGATGGCACAGGAGGAA	GCCCGTAGTGCTTCAGCTT
Slc6a8	GTGTGGAGATCTTCCGCCAT	CCCGTGGAGAGCCTCAATAC
Ucp1	AAGCTGTGCGATGTCCATGT	AAGCCACAAACCCTTTGAAAA

Cloning and generation of adenoviral knockdown constructs for expression in brown adipocytes

Complementary DNA oligos for shRNA generation were annealed and cloned into the pENTRTM/U6 entry vector according to the manufacturer's instructions (Invitrogen; K4944). Sequences used for shRNA targeting were as follows:

sh*Ckb*-#1 sense: CAC CGC GAG GAG AGT TAC GAC GTA TTC GAA AAT ACG TCG TAA CTC TCC TCG; antisense: AAA ACG AGG AGA GTT ACG ACG TAT TTT CGA ATA CGT CGT AAC TCT CCT CGC
sh*Ckb*-#2 sense: CAC CGC ACA ATG ACA ATA AGA CTT TCG AAA AAG TCT TAT TGT CAT TGT GC; antisense: AAA AGC ACA ATG ACA ATA AGA CTT TTT CGA AAG TCT TAT TGT CAT TGT GC
sh*LacZ* sense: CAC CGC TAC ACA AAT CAG CGA TTT CGA AAA ATC GCT GAT TTG TGT AG; antisense: AAA ACT ACA CAA ATC AGC GAT TTT TCG AAA TCG CTG ATT TGT GTA GC.

Cloned shRNA's were shuttled from the entry plasmid to the pAD/BLOCK-iT^{TM}-DEST Gateway® vector and transfected into 293A cells. Crude adenovirus was amplified by consecutive infection of 293 cells until ten, 15-cm dishes were attained. When 293A cells became cytopathic, cells were harvested, subjected to iterative freeze-thawing and centrifuged at 3000 g for 15 minutes. The resulting supernatant, containing adenovirus, was used to infect the next set of 293A cells. Glycerol was added to a final concentration of 10% to the final extract of amplified adenovirus. Primary brown adipocytes were transduced with adenovirus (1/50 dilution) in the evenings of day1 and day 3 of brown adipocyte differentiation. Media was replenished the following mornings.

Cloning, site-directed mutagenesis, and generation of adenoviral overexpression constructs for expression in brown adipocytes

The open reading frame of mouse *Ckb* (NM_021273) was closed from a BAT cDNA library. *Ckb* cDNA was cloned into the pENTR^{TM}/D-TOPO® vector using the pENTR Directional TOPO cloning kit following the manufacturers instructions (Invitrogen, K2400-20). Site-directed mutagenesis primers used to generate the CKB^{C283S}.FLAG, CKB$^{C141/6S}$.FLAG and CKB$^{\Delta iMTS\text{-}L}$.FLAG are as follows:

CKB$^{C141/6S}$.FLAG

Fwd: 5'- CAG CAT CCG CGG CTT CAG TCT CCC CCC GCA CAG CAG CCG CGG GGA GCG - 3'

Rev: 5’ - CGC TCC CCG CGG CTG CTG TGC GGG GGG AGA CTG AAG CCG CGG ATG CTG - 3’

CKB^{C283S}.FLAG

Fwd: 5’- CTG GGC TAC ATC CTC ACA AGC CCA TCC AAC CTG GGC AC -3’

Rev: 5’- GTG CCC AGG TTG GAT GGG CTT GTG AGG ATG TAG CCC AG -3’

CKB$^{\Delta iMTS-L}$.FLAG

Fwd: 5’- CTA CGT GCT GAG CTC GGA AGT GGA GAC AGG CGA GAG CAT CGA GGG CTT CTG TCT CCC CCC -3’

Rev: 5’- GGG GGG AGA CAG AAG CCC TCG ATG CTC TCG CCT GTC TCC ACT TCC GAG CTC AGC ACG TAG -3’

*Nucleotides changed to generate variants are highlighted in red

Cloned cDNA’s were shuttled from the pENTR™/D-TOPO® vector to the pAD/CMV/V5-DEST Gateway® vector and transfected into 293 cells to generate crude adenovirus according to the manufacturer’s instructions (Invitrogen; V493-20). Crude adenovirus was amplified by consecutive infection of 293 cells until ten, 15-cm dishes were attained. When 293A cells became cytopathic, cells were harvested and subjected to iterative freezing and thawing. Following the third and final thaw, cell debris was pelleted by centrifugation at 3000 x g for 15 minutes. The resulting supernatant, containing adenovirus, was used to infect the next set of 293A cells. Glycerol was added to a final concentration of 10% to the final extract of amplified adenovirus and stored at -80°C. Primary brown adipocytes were transduced with adenovirus to reach endogenous expression levels (determined empirically for each adenoviral preparation) in the evening of day 3 of brown adipocyte differentiation. Media was replenished the following morning.

Animals

Mice were housed at 22°C under a 12-hr light/dark cycle and given free access to food and water. All experiments used age-matched (6-8 weeks) wild-type C57BL/6N male mice purchased from Charles River (strain code: 027). Animal experiments were

performed according to procedures approved by the Animal Resource Centre at McGill University and complied with guidelines set by the Canadian Council of Animal Care.

Western blotting

Samples were prepared in adipocyte lysis buffer supplemented with a cocktail of protease inhibitors (Roche) and lysates were centrifuged at 16,000 g for 10 min at 4°C. The resulting supernatant was collected and protein concentration was determined using the BCA assay (Pierce). Protein lysates were denatured in Laemmli buffer (60 mM Tris pH 6.8, 2% SDS, 10% glycerol, 0.05 % bromophenol blue, 0.7 M β-mercaptoethanol), resolved using SDS-PAGE and then transferred to a polyvinylidene difluoride (PVDF) membrane. Membranes were blocked using tris-buffered saline (TBS) containing 0.005% Tween-20 (TBS-T) containing 5% milk. Primary antibodies were diluted in TBS-T containing 5% BSA, and 0.02% NaN_3. After 60 min blocking, membranes were decorated with primary antibodies and incubated overnight at 4°C. For incubation with secondary antibody, anti-rabbit or anti-mouse HRP (Promega) were diluted 1:10,000 (v/v) in TBS-T containing 5% milk. Membranes were washed three times for 10 min using TBS-T following both primary and secondary antibody incubation. Blots were visualized using enhanced chemiluminescence Western blotting substrates (Bio-rad).

Prediction of iMTS-L

iMTS-L signals were predicted as previously described[131,151]. Briefly, multiple CKB sequences were generated by sequentially removing single amino acids from the N-terminus and submitted all sequences to TargetP[152] with options set to non-plant organism and without cut-off and cleavage-site prediction. The mitochondrial targeting prediction (mTP) scores were plotted against the corresponding amino acid position. A threshold mTP of 0.75 was used to define the presence of an iMTS-L.

Estimation of mitochondrial abundance in murine tissue

Whole tissue extracts and purified mitochondria were prepared from BAT, heart, and kidney of $CKB^{FLAG/+}$ mice. To determine the abundance of mitochondria, whole tissue and mitochondrial lysates were loaded on the same polyacrylamide gel and anti-FLAG blots were used for quantification of CKB.FLAG protein by densitometry using ImageJ software. Following densitometry analysis, the total amount of CKB.FLAG was estimated by multiplying the densitometric value by the total amount of protein within the given extract (whole tissue or mitochondrial). Contamination of non-mitochondrial proteins in mitochondrial extracts was predicted based on VCL densitometry and subtracted from the mitochondrial signal. Subtraction of VCL-based contamination did not significantly alter the results due to the high quality of mitochondrial purification. The percentage of CKB.FLAG in mitochondria was calculated by dividing the total mitochondrial pool to the total amount of CKB in whole tissue lysates.

Creatine kinase activity assays

Creatine kinase activity (PCr generation) was determined using a coupled reaction utilizing pyruvate kinase and lactate dehydrogenase. Absorbance at 340 mM was measured to assess rate of ATP turnover using the kinetic setting on a VarioSKAN plate reader. The assay was performed at 25°C under the following conditions: 5 mM ATP, 4 mM PEP, 20 mM $MgCl_2$, 100 mM KCl, 0.45 mM NADH, 50 mM Tris pH 9, and 10 mM creatine. Approximately 100 µg of protein was used to determine creatine kinase activity in whole cell, post-mitochondrial supernatant, or mitochondrial extracts obtained from brown adipocytes.

Statistical analyses

Data were shown as mean ± s.e.m. One-way ANOVA were used to calculate *P* values in order to determine statistical differences. Significance was considered $p < 0.05$. *n* values

represent biological replicates for isolated mitochondria or cultured cell experiments and are detailed in the respective figure legend.

IV. RESULTS

CKB is regulated by cold selectively in BAT

It has previously been shown that creatine stimulates respiration through a futile cycle of phosphorylation/dephosphorylation in mitochondria of thermogenic adipocytes. Moreover, it has been demonstrated that loss of adipocyte creatine leads to reduced whole-body energy expenditure and diet-induced obesity in mice, in line with a thermogenic role for creatine cycling. There are four creatine kinase isoenzymes: CKB, CKM, CKMT1, and CKM2. Preliminary data from our laboratory suggests that CKB controls creatine cycling in brown adipocytes as CKB generates the vast majority of PCr in these cells and loss of *Ckb* leads to blunted rates of oxygen consumption in murine brown adipocytes. However, the thermogenic regulation of CKB has never been examined in brown fat.

The canonical thermogenic protein, UCP1, is regulated by environmental temperature and robustly increases in response to cold. To investigate whether CKB in brown fat is under a similar physiological regulation, wild-type (C57BL/6N) mice were first acclimated to thermoneutral (30°C) housing and then transferred to the cold (6°C) for various times. Thermoneutrality is the temperature at which core body temperature is maintained in the absence of sympathetic stimuli. RT-qPCR analysis of BAT showed that *Ckb mRNA* was significantly increased following 48 hours in the cold. Interestingly, the increase in *Ckb* was more dramatic than that of the known thermogenic effector, *Ucp1* (Fig. 1a). Western blotting of BAT protein lysates similarly displayed a dramatic increase in CKB protein levels by 48 hours of cold exposure and these levels were sustained when mice were housed for one week in the cold (Fig. 1b). The augmentation of CKB was independent of general increased protein synthesis as there was only a slight increase in other proteins blotted for including mitochondrial proteins (LONP1, HSP60, ATP5A) and the cytosolic protein, GAPDH (Fig. 1b and Fig. 1d). Moreover, these effects were only noticeable by Western blot when mice were housed for 7 days in the cold, whereas CKB induction was apparent by 48 hours of cold exposure. Notably, of every protein analyzed, the cold-mediated induction of CKB levels appeared to be the most dramatic in whole

BAT lysates. Expression of *Ckm* and *Ckmt2,* were unaltered in BAT following cold exposure whereas *Ckmt1* was increased approximately four-fold (Fig. 1c). In line with mRNA expression, Western blotting revealed protein bands cross-reacting with anti-CKM antibodies were also unchanged by cold (Fig. 1d). Expression of CKMT1 and CKMT2 were unable to be detected by Western blotting, presumably because expression of these enzymes is low in this tissue (data not shown).

Brown adipocytes are the functional unit of BAT, but brown fat is a highly heterogeneous tissue composed of many other cell types including endothelial cells (which line the capillaries), various immune cell populations, and preadipocytes (which can divide and differentiate into mature adipocytes under various stimuli). These other cell populations are collectively known as the stromal vascular fraction (SVF) and can be separated from mature brown adipocytes using an established technique to float and isolate mature fat cells from the less buoyant SVF. Floated adipocytes isolated from cold-exposed mice demonstrated that the cold-induced increase in CKB occurred within the purified brown adipocytes themselves (Fig. 1e).

Cold is a potent activator of beige adipocytes, inducing UCP1 expression and increasing respiration in this cell type[153,154]. In addition to UCP1-mediated thermogenesis, previous studies have shown that beige adipocytes exhibit thermogenic creatine cycling[96]. To ascertain whether CKB is also cold-regulated in beige adipocytes, Western blots were conducted using protein lysates prepared from inguinal fat pads of cold-exposed and thermoneutral-housed mice. Inguinal fat is the subcutaneous white fat depot that exhibits the greatest capacity for browning in mice[155,156]. Surprisingly, Western blotting showed that cold exposure did not affect CKB levels in inguinal fat extracts from cold-exposed mice despite robust increase in UCP1 levels, indicating that beige adipocyte recruitment did in fact result from cold exposure (Fig. 1f). Since CKB is normally studied in the context of the brain and is highly expressed in this tissue, the levels of CKB in the brain following cold exposure was also examined. Like inguinal fat, cold exposure had no effect on CKB levels in whole brain tissue lysates (Fig. 1g), suggesting that CKB induction following cold exposure is not a universal regulatory feature of CKB but instead is selective to BAT.

CKB levels are regulated by β3-adrenergic receptor signaling

Norepinephrine is released from sympathetic nerves and is the most potent physiological activator of brown fat thermogenesis in mice[157]. NE is thought to act primarily through activation of the β3-adrenergic receptor and downstream signaling pathways that lead to expression of a thermogenic gene program[158,159]. To investigate the role of β3-adrenergic receptor signaling on CKB expression, wild-type mice were injected intraperitoneally with CL316,243 (CL), a synthetic agonist specific for the β3-adrenergic receptor subtype. Stimulation of the β3-adrenergic receptor markedly increased CKB protein levels in brown fat (Fig. 2a). As expected, UCP1 levels were also significantly raised in BAT following treatment with CL (Fig. 2a).

Intriguingly, CKB levels were upregulated to a greater extent following cold exposure compared to β3-adrenergic receptor stimulation alone (compare induction of CKB in Fig. 2a to Fig. 1b and/or Fig. 2b), raising the possibility that there is input distinct from β3-adrenergic receptor signaling that contributes to CKB regulation upon sympathetic stimulation (i.e. cold exposure). One possibility is that NE acts on and induces signaling through a different subset(s) of adrenergic receptors present on the surface of brown adipocytes. To probe this idea further and to determine if the other β-adrenergic receptors play a role in regulating CKB levels, mice were administered propranolol, a non-selective β1- and β2-adrenergic receptor antagonist, and then subjected to cold exposure. Inhibition of β1- and β2-adrenergic receptors was insufficient to prevent the elevation of CKB in BAT of cold-exposed mice (Fig. 2b). Moreover, propranolol had no effect on cold-induced UCP1 levels in BAT (Fig. 2b). These data suggest that of all three β-adrenoceptors, only activation of the β3-adrernegic receptor subtype plays a role in regulating brown fat CKB levels, at least in mice.

Studies dating back to the 1980's suggest that signaling through the α1-adrenergic receptor supports BAT thermogenesis through a still unidentified mechanism[160,161]. Mining of independent data revealed that adipose expression of *Adra1a*, but not *Adra1b* and *Adra1d*, is restricted to the brown fat depot in mice (Fig. 2c), prompting determination of whether α-adrenoceptor signaling contributes to brown fat CKB regulation. Treating

mice with the α-adrenoceptor antagonist phenoxybenzamine significantly impaired CKB induction following cold exposure compared to vehicle-treated mice (Fig. 2d), and this inhibition was also observed at the mRNA level (Fig. 2e). Conversely, inhibition of α-adrenoceptor receptor signaling had no effect on *Ucp1* mRNA levels or UCP1 protein expression (Fig 2d. and Fig. 2e), suggesting that phenoxybenzamine was not exerting these effects through off-target β3-adrenergic receptor stimulation. Calcium cycling is another recently identified thermogenic mechanism present in adipocytes. This pathway is thought to be mediated by *Ryr2* and *Atp2a* and is stimulated by α-adrenoceptor receptor signaling[95]. However, neither cold nor inhibition of α-adrenoceptor signaling had any effect on the levels of *Ryr2* or *Atp2a* transcripts in mice (Fig. 2e). Together, these results confirm a role for canonical β3-adrenergic receptor signaling in brown fat regulation of CKB but also suggest that activation of α-adrenoceptors may be required for full induction of CKB levels following thermogenic stimuli.

Stimulation of α1-adrenoceptors increases CKB levels in primary brown adipocytes

An *in vitro* cellular system was next used to further interrogate the role of α-adrenoceptor signaling in regulation of CKB levels in brown fat. Primary brown adipocytes were treated with various pharmaceutical agonists specific for different subsets of adrenoceptors. In contrast to *in vivo* results, CKB levels were unchanged in primary brown adipocytes treated with CL or norepinephrine despite increased lipolytic signaling as demonstrated by enhanced levels of phosphorylated HSL and indicative of successful activation of β-adrenoceptor signaling (Fig. 3a and Fig. 3b). Similarly, treating primary brown adipocytes with isoproterenol, a β1- and β2-adrenergic receptor agonist, had no effect on CKB levels despite a small dose-dependent increase in phosphorylated HSL (Fig. 3c).

Interestingly, only the α1-adrenergic receptor agonist, phenylephrine, was able to elicit an increase in CKB, but the observed effect was minimal (Fig 3d). Previous studies have demonstrated that α1-adrenergic receptor signalling leads to extracellular signal-regulated kinase (ERK) activation and phosphorylation in some cell types[162]. However,

there was no observable effect on ERK phosphorylation when brown adipocytes were treated with phenylephrine (Fig. 3d). On the contrary, there was a slight increase in HSL phosphorylation (Fig. 3d), which is surprising since, to our knowledge, HSL is not thought to be a downstream target of α-adrenoceptor signaling. However, as levels of total HSL were not examined, the increase in phosphorylated HSL following phenylephrine could just be the result of increased total HSL levels. Taken together, these data are intriguing given that each pharmaceutical agent appeared to induce HSL phosphorylation, but only phenylephrine was able to increase CKB levels (albeit modestly). These observations suggest that supposed activation of α-adrenoceptors through phenylephrine agonism regulates CKB levels in brown adipocytes through a mechanism that we have so far been unable to delineate.

CKB is localized to brown adipocyte mitochondria

The above data suggest a role for CKB in brown adipocyte creatine-dependent thermogenesis. This is surprising given that CKB is typically described and thought of as a cytosolic protein; moreover, creatine cycling has been demonstrated in isolated mitochondria. In line with thus, unpublished quantitative proteomic data from our lab revealed that CKB is the most abundant creatine kinase isoenzyme in crude mitochondria isolated from murine primary brown adipocytes. To further investigate mitochondrial localization of CKB and examine whether CKB is stably imported into the organelle, mitochondria were purified from primary (wild-type) or immortalized *Ckb*$^{fl/fl}$ and *Ckb*$^{-/-}$ brown adipocytes and subjected to protease (trypsin) treatment. Protease treatment of mitochondrial extracts is a well-established method for assessing stable import and internalization of mitochondrial proteins[163-166]. Briefly, trypsin degrades non-internalized proteins including outer mitochondrial membrane receptors and endoplasmic reticulum proteins (that are often co-purified with mitochondria), whereas stably imported mitochondrial proteins are resistant to trypsin degradation. Endogenous CKB was protected from proteolysis in mitochondrial extracts isolated from primary brown adipocytes (Fig. 4a). Moreover, a protease-protected band cross-reacting with anti-CKB was enriched in *Ckb*$^{fl/fl}$ compared to *Ckb*$^{-/-}$ immortalized brown adipocytes (Fig. 4b).

UCP1, ETC proteins (ATP5A, UQCRC2, MTCOI, SDHB, NDUFB8), and the matrix protein LONP1, were also shielded from proteolysis (Fig. 4a and Fig. 4b). Conversely, TOM20, an outer mitochondrial membrane import receptor, and Calnexin, an endoplasmic reticulum integral membrane protein, were completely degraded in the presence of trypsin (Fig. 4a). Importantly, all mitochondrial proteins, including CKB, were degraded in the presence of the detergent Triton X-100, indicating that permeabilization of mitochondrial membranes yields CKB (and all mitochondrial internalized proteins) vulnerable to trypsin proteolysis (Fig. 4a and Fig. 4b). To establish whether CKB is targeted to brown fat mitochondria *in vivo*, BAT mitochondria were isolated from wild-type mice subjected to either thermoneutral or cold temperature (6°) housing. CKB levels were increased in protease-treated mitochondrial extracts from BAT following 48 hours of cold-exposure and were further increased upon 7 days in the cold (Fig. 4c). These data indicate that CKB is partitioned to mitochondria both *in vitro* and *in vivo*.

To further validate CKB as a mitochondrial protein, CRISPR/Cas9 technology was used to generate mice expressing CKB with a carboxy-terminus FLAG epitope tag from the endogenous *Ckb* locus (*Ckb*^{FLAG} mice) (Fig. 4d). *Ckb*^{FLAG} mice enabled the use of commercially available antibodies directed against FLAG to monitor endogenous CKB levels. Like wild-type mice, CKB.FLAG protein levels were dramatically upregulated in BAT of heterozygous *Ckb*$^{FLAG/+}$ mice when subjected to cold exposure (6°C) for 48 hours (Fig. 4e). Importantly, insertion of a FLAG tag did not impair CKB induction, as wild-type CKB and CKB.FLAG were induced to a similar extent upon cold exposure in *Ckb*$^{FLAG/+}$ mice (Fig. 4e). Comparing mitochondria from wild-type and CKB.FLAG mice confirmed the presence of CKB.FLAG co-localization with known mitochondrial proteins (Fig. 4f). Importantly, trypsin treatment resulted in degradation of TOM70, Calnexin, and the polysome protein, PMP70. Conversely, CKB, LONP1, and components of the ETC were all protected from proteolysis, implying that these proteins are stably imported into the organelle. Next, mitochondrial abundance of CKB was compared between known CKB-expressing tissues in room-temperature housed CKB.FLAG mice. Interestingly, approximately 10% of the total CKB pool in BAT was internalized into mitochondria, while less than 1% of total CKB was found in protease-treated mitochondrial extracts from the kidney and heart tissues (Fig. 4g and Fig. 4h).

The mitochondrial targeting sequence of CKB is not contained with the first 40 amino acids or within the CX_4C cysteine motif

CKB is not annotated as a mitochondrial enzyme and thus, the targeting signal(s) that directs CKB to mitochondria is not known. To directly test whether the canonical open reading frame of CKB contains a mitochondrial targeting signal, adenoviral constructs of carboxy-terminus Flag-tagged CKB (CKB^{WT}.FLAG) were generated for overexpression in brown adipocytes (Fig. 5a). Protease protection assays revealed that CKB^{WT}.FLAG as well as LONP1 were both completely protected from trypsin degradation in mitochondrial extracts prepared from primary brown adipocytes differentiated *in vitro* (Fig. 5d). Importantly, TOM20 was completely degraded in the presence of trypsin, indicating efficient degradation of non-stably imported proteins in protease-treated samples (Fig. 5d). These data indicate that the open reading frame of CKB harbours a signal that is sufficient for targeting and translocation into brown adipocyte mitochondria.

Analysis of the primary amino acid sequence of CKB revealed that CKB does not contain a canonical N-terminal MTS that is characteristic of many mitochondrial proteins. Nonetheless, to establish whether the N-terminus of CKB is important for mitochondrial targeting, we constructed adenovirus expressing a variant of CKB lacking the first 40 amino acids of the primary sequence ($CKB^{\Delta 1\text{-}40}$.FLAG) (Fig 5b). Since truncation of the first 40 codons would yield a transcript lacking a proper start codon, a typical AUG start codon was cloned into the open reading frame of $CKB^{\Delta 1\text{-}40}$.FLAG (Fig. 5b). Adenoviral expression of $CKB^{\Delta 1\text{-}40}$.FLAG in brown adipocytes yielded a truncated protein that was resistant to proteolysis in mitochondrial extracts treated with trypsin (Fig.5d and Fig. 5e). Importantly, the truncated $CKB^{\Delta 1\text{-}40}$.FLAG variant resulted in a longer migration distance during SDS-PAGE, confirming specificity of the CKB.FLAG protein band. Though the Western blot in Figure 5e shows that the $CKB^{\Delta 1\text{-}40}$.FLAG variant runs very close to the non-specific band, there is clearly a specific CKB.FLAG band in the protease-treated lane, indicating stable import of this variant.

Further analysis of CKB primary sequence revealed the presence of an atypical cysteine motif represented as two cysteine residues separated by four amino acids (a single CX_4C motif). This sequence spans amino acid residues 141 to 146 and is a

possible substrate for Mia40-dependent mitochondrial protein import[167,168]. To determine if the CX_4C motif of CKB is important for mitochondrial targeting and translocation, the potential interaction between Mia40 and CKB was disrupted by replacing each cysteine residue of the CX_4C motif with a serine residue ($CKB^{C141/6S}$.FLAG) using site-directed mutagenesis (Fig. 5c). Serine was chosen to replace cysteine as it is the most structurally similar amino acid to cysteine but lacks the ability to form disulfide bonds. $CKB^{C141/6S}$.FLAG was completely protected from trypsin degradation in mitochondrial extracts from primary brown adipocytes (Fig. 5d), suggesting that CKB mitochondrial translocation is not dependent on the CX_4C motif present in CKB and is likely independent of Mia40. Western blotting of whole cell extracts from brown adipocytes showed similar expression between each CKB.FLAG variant (Fig. 5e). Together, these data demonstrate that neither the N-terminus nor CX_4C motif of CKB confer mitochondrial targeting.

CKB is targeted to mitochondria through an iMTS-L

It has recently been demonstrated that the TOM70 import receptor mediates and/or enhances mitochondrial protein import through internal matrix targeting signal-like (iMTS-L) present in substrate proteins[131]. These iMTS-L exhibit similar characteristics to canonical N-terminal MTS, such as increased frequency of lysine, arginine, and hydroxylated residues (serine, threonine), as well as increased propensity to form amphipathic alpha helices[131]. The TargetP algorithm is trained on sets of proteins with known cellular localization and can predict mitochondrial targeting (based on presence or absence of a N-MTS) with high accuracy[152]. The primary sequence of CKB was consecutively truncated by a single amino acid residue and each resulting sequence was submitted to TargetP, a previously established method of identifying iMTS-L by plotting the predicted MTS value against the corresponding residue[169]. Using this method, CKB was predicted to contain a strong (0.8 TargetP score) iMTS-L spanning amino acids ~130 - 140 (Fig. 6a). A closer look at this region revealed the presence of four arginine residues within the putative iMTS-L of CKB. Computational analysis predicted that mutation of each arginine residue to glutamate would abolish the putative targeting signal (Fig. 6a). The amino acid changes were generated using site-directed mutagenesis ($CKB^{\Delta iMTS-}$

^{L}.FLAG) for overexpression in brown adipocytes through an adenovirus vector (Fig. 6b). CKB$^{\Delta iMTS\text{-}L}$.FLAG was degraded in trypsin-treated mitochondrial extracts from *Ckb*$^{-/-}$ brown adipocytes, whereas CKB^{WT}.FLAG and an enzymatically defective variant, CKB^{C283S}.FLAG, were completely protected from proteolysis in the same cells (Fig. 6c). In line with these observations, CKB^{WT}.Flag was able to fully restore creatine kinase activity in protease-treated mitochondrial extracts from *Ckb*$^{-/-}$ brown adipocytes (Fig. 6d). Conversely, overexpression of GFP.FLAG, CKB$^{\Delta iMTS\text{-}L}$.FLAG or CKB^{C283S}.FLAG had no effect on mitochondrial creatine kinase activity in *Ckb*$^{-/-}$ brown adipocytes (Fig. 6d).

Importantly, Western blotting of whole cell extracts and post-mitochondrial supernatants (also known as the cytosolic fraction) showed similar expression levels of each CKB.FLAG variant in *Ckb*$^{-/-}$ brown adipocytes (Fig. 6f and Fig. 6g). Moreover, *in vitro* creatine kinase assays revealed no difference in cytosolic creatine kinase activity in *Ckb*$^{-/-}$ brown adipocytes expressing CKB^{WT}.FLAG or CKB$^{\Delta iMTS\text{-}L}$.FLAG (Fig. 6h). Conversely, no creatine kinase activity was detected in cytosolic extracts from *Ckb*$^{-/-}$ brown adipocytes expressing GFP.FLAG or CKB^{C283S}.FLAG (Fig. 6h). Taken together, these data imply that CKB mitochondrial targeting information is contained within an iMTS-L and that mutation of arginine residues in this sequence hinders mitochondrial internalization of CKB.

Identifying the presence of a functional iMTS-L sequence in CKB prompted us to determine whether mitochondrial CKB import is dependent on TOM70. Immortalized *Ckb*$^{fl/fl}$ and *Ckb*$^{-/-}$ brown adipocytes were transduced with adenovirus expressing shRNA targeted against *Tom70* or *LacZ* as a control. CKB levels appeared unchanged in protease-treated mitochondrial extracts from TOM70-deficient brown adipocytes (Fig. 6i). These results warrant further research but initially suggest that mitochondrial import of CKB may be independent of TOM70.

CKB internalization into mitochondria is cell-type dependent

We previously established that a low proportion (< 1%) of endogenous CKB.FLAG was found in mitochondria purified from murine heart and kidney of CKB$^{FLAG/+}$ mice. Since mitochondrial localization of CKB appears to be mediated by an iMTS-L, we next set out to determine whether overexpression of the CKB open reading frame (CKB^{WT}.FLAG) was

sufficient for mitochondrial targeting in other cell types *in vitro*. Like previously demonstrated, protease protection assays demonstrated that CKB^{WT}.FLAG and other known mitochondrial proteins, TIM23 and TFAM, were internalized into mitochondria purified from primary brown adipocytes (Fig. 7a). Conversely, mitochondria purified from primary brown preadipocytes revealed that a significant portion of CKB^{WT}.FLAG protein was degraded in protease-treated mitochondrial extracts (Fig. 7b). As expected, levels of the mitochondrial and matrix proteins, TIM23 and TFAM respectively, were similar between untreated and protease-treated organelles, indicating that known mitochondrial proteins were stably imported into the organelle. Similar to CKB^{WT}.FLAG, TOM20, Calnexin, and PMP70 were largely degraded in the presence on trypsin (Fig. 7b). In mouse embryonic fibroblasts (MEFs), CKB^{WT}.FLAG and TIM23 levels were slightly reduced in protease-treated mitochondrial extracts from mouse embryonic fibroblasts (MEFs) overexpressing CKB^{WT}.Flag (Fig. 7c). Conversely, TFAM levels remained unchanged whereas TOM20, Calnexin, and PMP70 were completely degraded in the presence of trypsin (Fig. 7c). Similar to observations in primary brown adipocytes, CKB^{WT}.FLAG, TIM23, and TFAM levels were unchanged in untreated and protease-treated mitochondrial extracts from primary murine white adipocytes from inguinal fat, signifying stable import of CKB^{WT}.Flag in these cell types (Fig. 7d).

The levels of CKB^{WT}.FLAG overexpression at the whole cell level in primary brown and white adipocytes, as well as MEFs was determined by Western blotting. Expression of CKB^{WT}.FLAG in primary brown preadipocytes was too high to determine the levels of CKB^{WT}.FLAG in the other cell types when ran on the same gel and thus, was excluded from these blots. Of the cell types examined, CKB^{WT}.FLAG was most highly expressed in MEFs, followed by median expression in primary brown adipocytes and relatively low expression of CKB^{WT}.FLAG in primary white adipocytes (Fig. 7e). Despite expressing CKB^{WT}.FLAG most abundantly in whole cell extracts, CKB^{WT}.FLAG could not be detected in MEF mitochondrial extracts when compared side-by-side with CKB^{WT}.FLAG levels in mitochondria purified from primary brown and white adipocytes (Fig. 7f). Surprisingly, primary white adipocytes express higher levels of endogenous CKB compared to brown adipocytes (Fig. 7e), though similar amounts of endogenous CKB were present in protease-treated mitochondrial extracts from both of these cell types (Fig. 7f). Taken

together with previous observations, these data suggest that despite harbouring an iMTS-L in the primary sequence, mitochondrial localization of endogenous CKB seems to be enhanced in brown adipocytes.

V. FIGURES

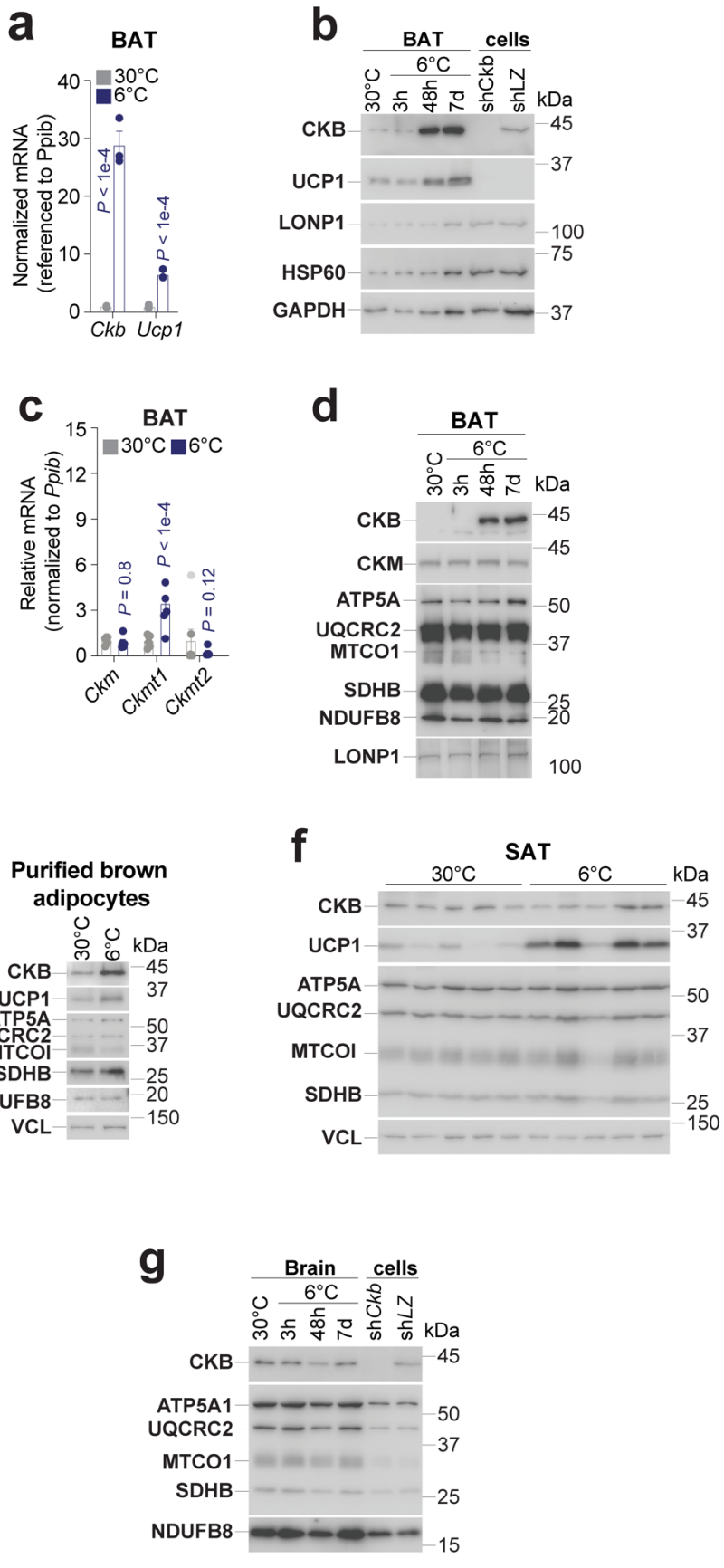
a
BAT
30°C
6°C
Normalized mRNA (referenced to Ppib)
P < 1e-4
P < 1e-4
Ckb
Ucp1
b
BAT
cells
6°C
30°C
3h
48h
7d
shCkb
shLZ
kDa
CKB
UCP1
LONP1
HSP60
GAPDH
45
37
100
75
37
c
BAT
30°C
6°C
Relative mRNA (normalized to Ppib)
P = 0.8
P < 1e-4
P = 0.12
Ckm
Ckmt1
Ckmt2
d
BAT
6°C
30°C
3h
48h
7d
kDa
CKB
CKM
ATP5A
UQCRC2
MTCO1
SDHB
NDUFB8
LONP1
45
45
50
37
25
20
100
e
Purified brown adipocytes
30°C
6°C
kDa
CKB
UCP1
ATP5A
UQCRC2
MTCOI
SDHB
NDUFB8
VCL
45
37
50
37
25
20
150
f
SAT
30°C
6°C
kDa
CKB
UCP1
ATP5A
UQCRC2
MTCOI
SDHB
VCL
45
37
50
37
25
150
g
Brain
cells
6°C
30°C
3h
48h
7d
shCkb
shLZ
kDa
CKB
ATP5A1
UQCRC2
MTCO1
SDHB
NDUFB8
45
50
37
25
15

Figure 1. CKB is regulated by cold selectively in BAT

(a) RT-qPCR analysis of *Ckb* and *Ucp1* transcript levels from BAT of wild-type male mice (C57BL6/N, 6-8 weeks of age). Animals were reared at 23°C, transferred to single-housing at 30°C for five days, and then maintained at 30°C or subjected to 6°C or 48 hours (*n*= 3 per group). mRNA levels were normalized to expression of the housekeeping gene, *Ppib.* **(b)** Western blot of protein lysates extracted from BAT of wild-type male mice. Animals were reared at 23°C, transferred to single-housing at 30°C for five days, and then subjected to 30°C or 6°C for various times. GAPDH was used as a loading control and known mitochondrial proteins (LONP1, HSP60) were used as markers of mitochondrial abundance. UCP1 was used to demonstrate thermogenic activation of BAT. Primary brown adipocytes infected with shRNA targeting *LacZ* (sh*LZ*) or *Ckb* (sh*Ckb*) were used to demonstrate specificity of the anti-CKB antibody. **(c)** RT-qPCR analysis of *creatine kinase isoenzyme* transcript levels from BAT of wild-type male mice. Animals were reared at 23°C, transferred to single-housing at 30°C for five days, and then maintained at 30°C or subjected to 6°C or 48 hours (*n*= 3 per group). **(d)** Western blot of protein lysates extracted from BAT of wild-type male mice. Animals were reared at 23°C, transferred to single-housing at 30°C for five days, and then subjected to 30°C or 6°C for various times. **(e)** Western blot of mature brown adipocyte lysates purified from BAT of wild-type male mice that were reared at 23°C, transferred to single-housing at 30°C for five days, and then subjected to 30°C or 6°C for 48 hours. Blotting of ETC components (ATP5A, UQCRC2, MTCO1, SDHB, NDUFB8) were used as markers of mitochondrial abundance. **(f)** Western blot of inguinal SAT from wild-type male mice. Animals were reared at 23°C, transferred to single-housing at 30°C for five days, and then subjected to 30°C or 6°C or 48 hours. **(g)** Western blot of protein extracts from brain of wild-type male mice. Animals were reared at 23°C, transferred to single-housing at 30°C for five days, and then subjected to 30°C or 6°C for various times.

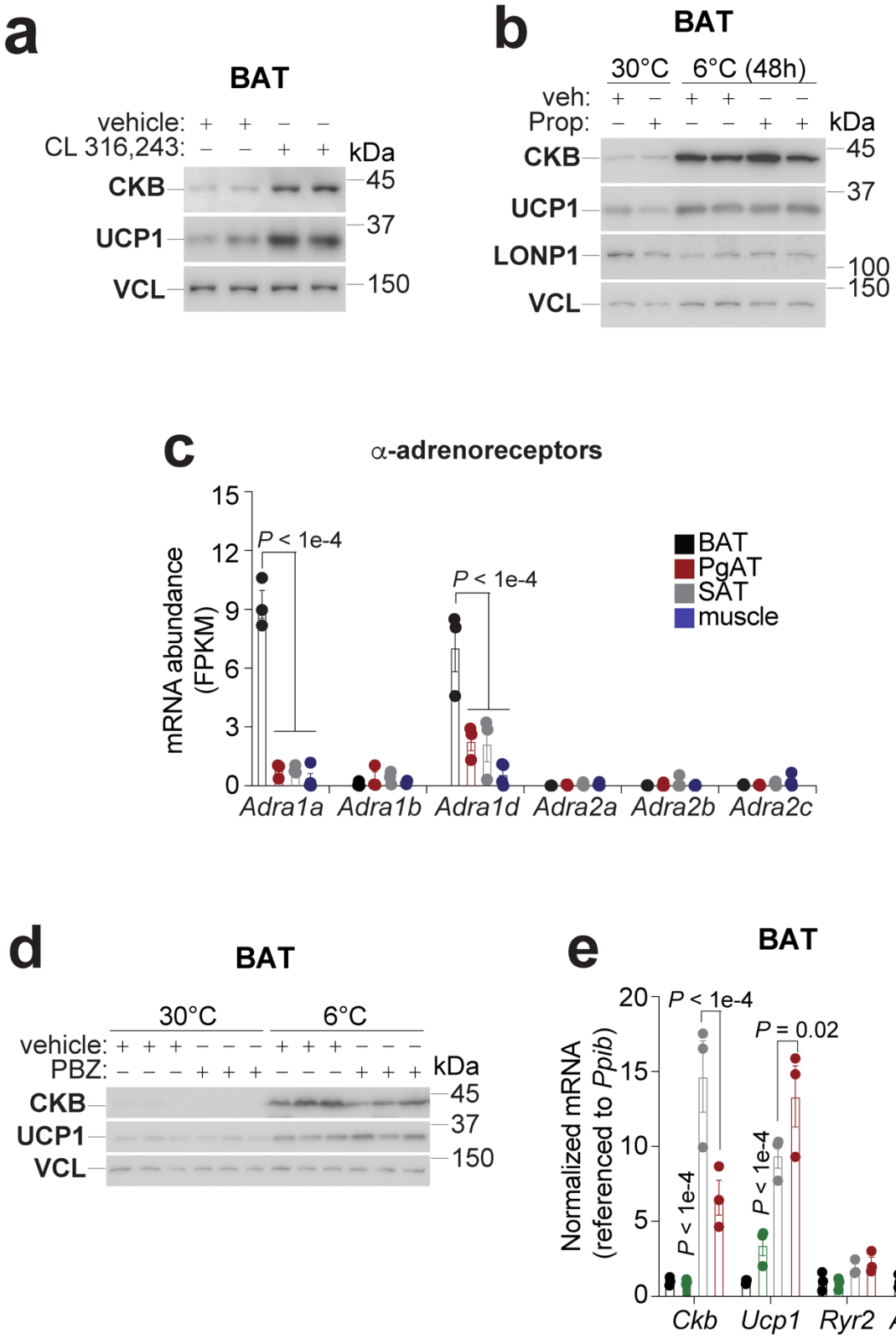
a
BAT
vehicle: + + – –
CL 316,243: – – + +
kDa
CKB
UCP1
VCL
45
37
150
b
BAT
30°C
6°C (48h)
veh: + – + + – –
Prop: – + – – + +
kDa
CKB
UCP1
LONP1
VCL
45
37
100
150
c
α-adrenoreceptors
mRNA abundance (FPKM)
15
12
9
6
3
0
P < 1e-4
P < 1e-4
BAT
PgAT
SAT
muscle
Adra1a
Adra1b
Adra1d
Adra2a
Adra2b
Adra2c
d
BAT
30°C
6°C
vehicle: + + + – – – + + + – – –
PBZ: – – – + + + – – – + + +
kDa
CKB
UCP1
VCL
45
37
150
e
BAT
Normalized mRNA (referenced to Ppib)
20
15
10
5
0
P < 1e-4
P = 0.02
P < 1e-4
P < 1e-4
30°C+veh
30°C+PBZ
6°C+veh
6°C+PBZ
Ckb
Ucp1
Ryr2
Atp2a2

Figure 2. CKB levels are regulated by β3-adrenergic receptor signaling

(a) Western blot of protein lysates prepared from BAT of wild-type mice. Animals were reared at 23°C, transferred to housing at 30°C for five days and then maintained at 30°C while subjected to intraperitoneal injection of CL 316,243 (CL, 1 mg/kg) or saline (veh.) once daily for two days. BAT was harvested two hours following the last injection of CL or veh. VCL was used as a loading control and UCP1 was used to demonstrate activation of β3-adrenergic receptor signaling by CL. **(b)** Western blot of protein lysates prepared from BAT of wild-type mice. Animals were reared at 23°C, transferred to housing at 30°C for 5 days and then maintained at 30°C or subjected to 6°C or 48 hours. For propranolol treatment, mice were injected intraperitoneally (5 mg/kg) once daily for 72 hours, starting one day before being transferred to cold. BAT was harvested two hours following the last injection with propranolol or saline (veh.) control. LONP1 was used to as a marker of mitochondrial abundance and UCP1 was used to demonstrate thermogenic activation of BAT by cold. **(c)** mRNA abundance, measured in Fragments Per Kilobase of transcript per Million mapped reads (FPKM), of α-adrenoceptor abundance in various adipose tissue depots from mice. Data were obtained from a publicly available RNA-seq data set from Long et al.[170] **(d)** Western blot of protein lysates or **(e)** RT-qPCR analysis of BAT from wild-type mice. Animals were reared at 23°C, transferred to housing at 30°C for 5 days and then maintained at 30°C or subjected to 6°C or 48 hours. For phenoxybenzamine (PBZ) treatment, mice were injected intraperitoneally (5 mg/kg) one hour prior to being transferred to the cold and once more 24 hours later. For mRNA analysis by RT-qPCR, mRNA levels were normalized to housekeeping gene, *Ppib*.

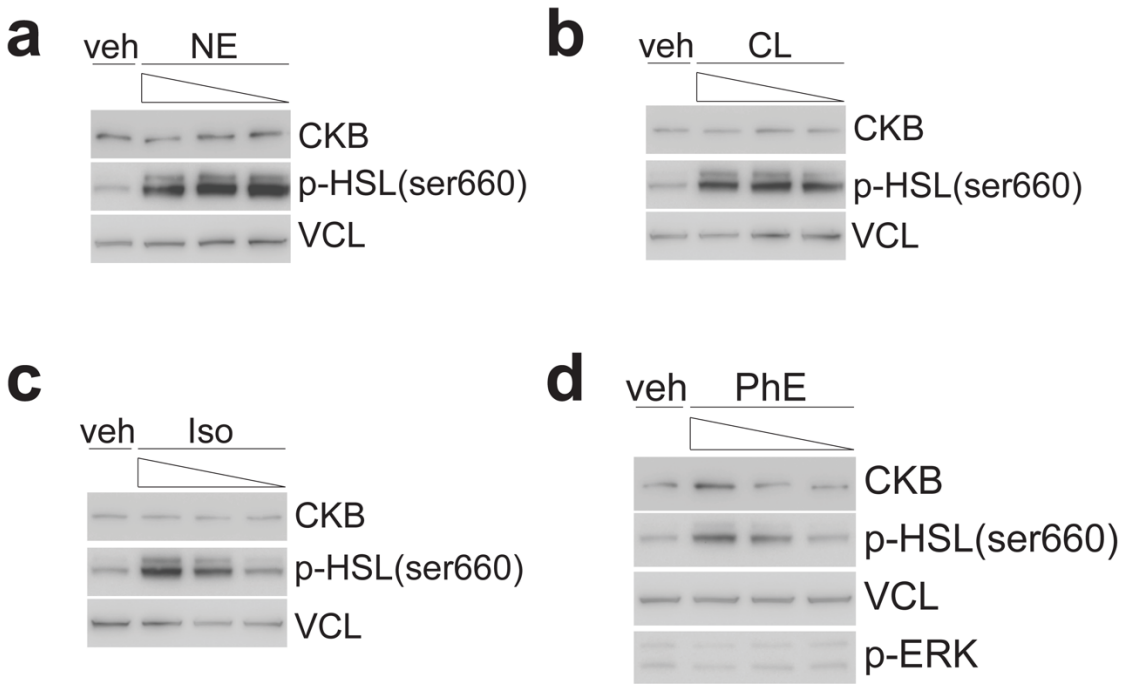

Figure 3. Stimulation of α1-adrenoceptors increases CKB levels in primary brown adipocytes

(a) Western blot of CKB in protein lysates prepared from primary brown adipocytes treated with 10, 1, or 0.1 μM norepinephrine, **(b)** 1, 0.1, or 0.01 μM CL-316,243 **(c)** 10, 1, or 0.1 μM isoproterenol, or **(d)** 10, 1, or 0.1 μM phenylephrine (PhE). For each condition, saline was used as a vehicle (veh) control. Blotting of phosphorylated HSL (p-HSL) was used to assess activation of β-adrenoceptor signaling and phosphorylated ERK (p-ERK) was used to determine activation of α-adrenoceptor signaling. Each treatment was initiated in the evening of day 6 differentiated primary brown adipocytes and cells were treated once again 12 hours later. Cells were harvested for protein 1 hour following the last treatment.

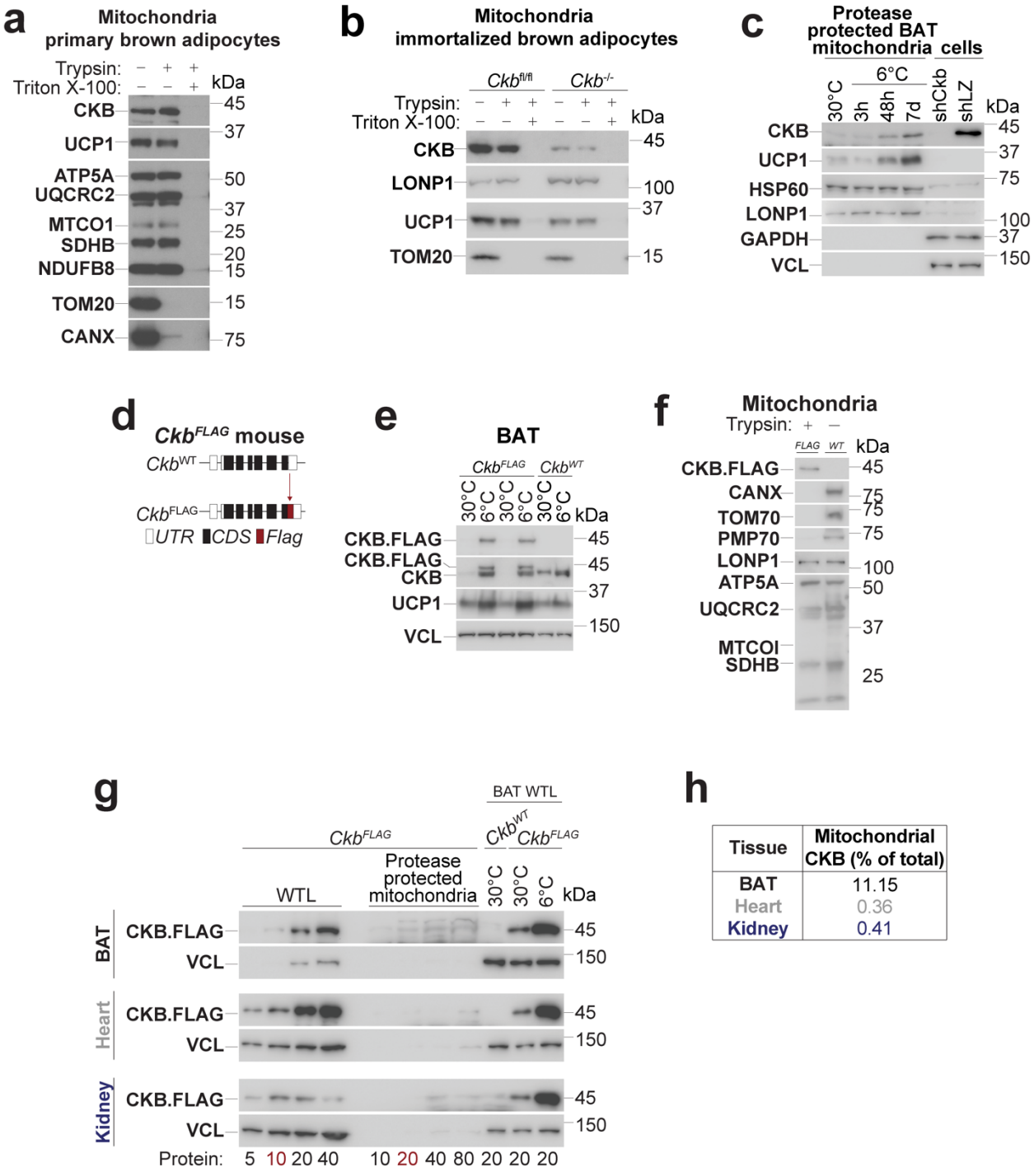

Tissue	Mitochondrial CKB (% of total)
BAT	11.15
Heart	0.36
Kidney	0.41

Figure 4. CKB is localized to brown adipocyte mitochondria

(a) Western blot of mitochondrial extracts from primary brown adipocytes differentiated *in vitro* with and without trypsin treatment. **(b)** Western blot of mitochondrial extracts from immortalized brown adipocytes differentiated *in vitro* with and without trypsin treatment. **(c)** Western blot of protease-treated mitochondrial extracts from male wild-type mice that were reared at 23°C and then transferred to single-housing at 30°C for 5 days. After five days, mice remained at 30°C or were subjected to 6°C for various times (*n*= 5 per group). Primary brown adipocytes infected with shRNA targeting *LacZ* (sh*LZ*) or *Ckb* (sh*Ckb*) were used to demonstrate specificity of the CKB antibody. **(d)** Schematic illustrating insertion of a Flag tag at the carboxy-terminus of the endogenous *Ckb* locus. UTR, untranslated region; CDS, coding sequence. **(e)** Western blot of protein lysates prepared from BAT of $Ckb^{FLAG/+}$ and wild-type mice. Animals were reared at 23°C and then transferred to single-housing at 30°C for 5 days and then subjected to 30°C or 6°C for 48 hours. Blots were probed with anti-CKB and anti-FLAG to demonstrate similar cold induction of both wild-type CKB and CKB.FLAG. UCP1 was used to validate cold-mediated activation of thermogenesis and VCL was used as a loading control. Each lane represents an individual mouse. **(f)** Western blot comparing protease-treated mitochondrial extracts from BAT of CKB^{FLAG} mice to untreated mitochondrial extracts from BAT of wild-type mice. CANX, TOM70, and PMP70 were used to demonstrate efficiency of trypsin degradation whereas LONP1 and ETC components were used to show protection of mitochondria-internalized proteins from proteolysis. **(g)** Western blot comparing CKB.FLAG protein levels in whole tissue lysates (WTL) and protease-treated mitochondria prepared from BAT, heart, and kidney from $CKB^{FLAG/+}$ mice. WTLs from wild-type and CKB^{FLAG} mice (last three lanes) were used to demonstrate specificity of the anti-FLAG antibody. Total amount of protein (μg) from each respective extract (WTL and protease-treated mitochondria) is indicated at the bottom. The lanes used for calculating the percentage of mitochondria from each tissue is highlighted in pink and used for **(h)** Percentage of mitochondrial CKB (% of total WTL) in each tissue examined. A detailed description of how mitochondrial percentage of CKB was calculated is outlined in the methods section.

a **CKB^{WT}.Flag**

MPFSNSHNTQKLRFPAEDEFPDLSSHNNHMAKVLTPELYAELRAKCTPSGFTLDDAIQTG
VDNPGHPYIMTVGAVAGDEESYDVFKDLFDPIIEERHGGYQPSDEHKTDLNPDNLQGGDDL
DPNYVLSSRVRTGRSIRGFCLPPHCSRGERRAIEKLAVEALSSLDGDLSGRYYALKSMTEA
EQQQLIDDHFLFDKPVSPLLLASGMARDWPDARGIWHNDNKTFLVWINEEDHLRVISMQKG
GNMKEVFTRFCTGLTQIETLFKSKNYEFMWNPHLGYILTCPSNLGTGLRAGVHIKLPHLGK
HEKFSEVLKRLRLQKRGTGGVGTAAVGGVFDVSNADRLGFSEVELVQMVVDGVKLLIEMEQ
RLEQGQAIDDLMPAQSDTAPGSQDYKDDDK

b **CKB$^{\Delta 1\text{-}40}$.Flag**

MELRAKCTPSGFTLDDAIQTG
VDNPGHPYIMTVGAVAGDEESYDVFKDLFDPIIEERHGGYQPSDEHKTDLNPDNLQGGDDL
DPNYVLSSRVRTGRSIRGFCLPPHCSRGERRAIEKLAVEALSSLDGDLSGRYYALKSMTEA
EQQQLIDDHFLFDKPVSPLLLASGMARDWPDARGIWHNDNKTFLVWINEEDHLRVISMQKG
GNMKEVFTRFCTGLTQIETLFKSKNYEFMWNPHLGYILTCPSNLGTGLRAGVHIKLPHLGK
HEKFSEVLKRLRLQKRGTGGVGTAAVGGVFDVSNADRLGFSEVELVQMVVDGVKLLIEMEQ
RLEQGQAIDDLMPAQSDTAPGSQDYKDDDK

c **CKB$^{C141/6S}$.Flag**

MPFSNSHNTQKLRFPAEDEFPDLSSHNNHMAKVLTPELYAELRAKCTPSGFTLDDAIQTG
VDNPGHPYIMTVGAVAGDEESYDVFKDLFDPIIEERHGGYQPSDEHKTDLNPDNLQGGDDL
DPNYVLSSRVRTGRSIRGFSLPPHSSRGERRAIEKLAVEALSSLDGDLSGRYYALKSMTEA
EQQQLIDDHFLFDKPVSPLLLASGMARDWPDARGIWHNDNKTFLVWINEEDHLRVISMQKG
GNMKEVFTRFCTGLTQIETLFKSKNYEFMWNPHLGYILTCPSNLGTGLRAGVHIKLPHLGK
HEKFSEVLKRLRLQKRGTGGVGTAAVGGVFDVSNADRLGFSEVELVQMVVDGVKLLIEMEQ
RLEQGQAIDDLMPAQSDTAPGSQDYKDDDK

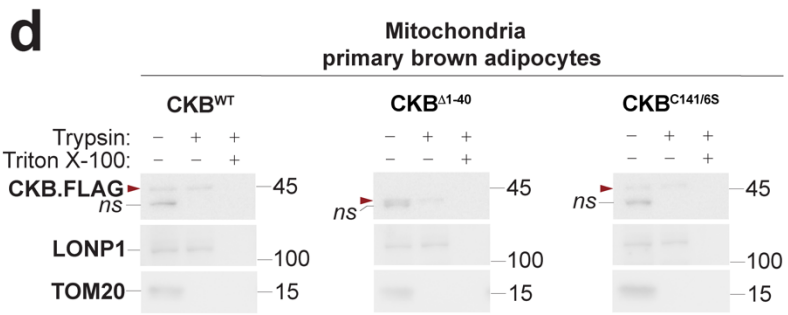

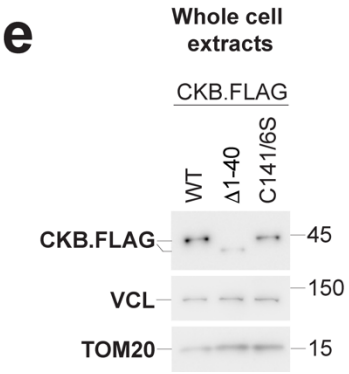

Figure 5. The mitochondrial targeting sequence of CKB is not contained with the first 40 amino acids or within the CX_4C cysteine motif

(a) Primary amino acid sequence of CKB^{WT}.FLAG. The linker sequence separating CKB from the FLAG tag is highlighted in grey and the FLAG epitope tag is highlighted in blue. **(b)** Primary amino acid sequence of $CKB^{\Delta 1\text{-}40}$.FLAG. A canonical methionine start codon was added to the beginning of the truncated protein for efficient translation and is highlighted in green. **(c)** Primary amino acid sequence of $CKB^{C141/6S}$.FLAG. The mutated residues are highlighted in red. **(d)** Western blot of purified mitochondrial extracts with and without trypsin treatment from primary brown adipocytes differentiated *in vitro*. TOM20 and LONP1 were used to show integrity of protease-protection assay. CKB.FLAG protein is denoted with a red arrow. ns, nonspecific. **(e)** Western blot of whole cell extracts from primary brown adipocytes used to purify mitochondria from (d).

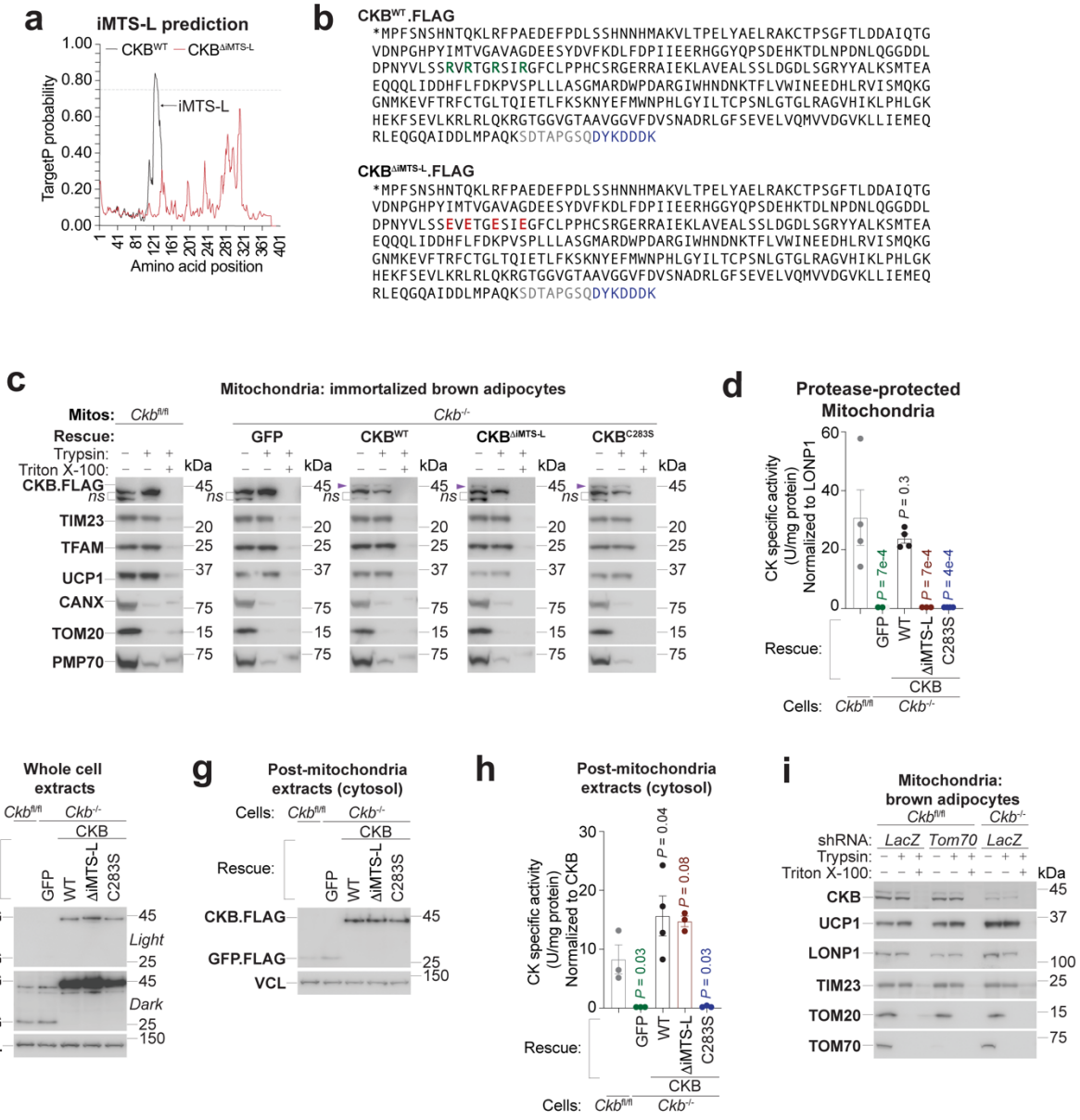

Figure 6. CKB is targeted to mitochondria through an iMTS-L

(a) The mitochondrial targeting prediction (mTP) score from TargetP analysis is plotted against the CKB amino acid sequence. A detailed description regarding how TargetP scores were obtained for each consecutive sequence can be found in the materials and methods section. **(b)** Primary amino acid sequence of CKB^{WT}.FLAG (top) and $CKB^{\Delta iMTS\text{-}L}$.FLAG. The four arginine residues mutated to glutamate are highlighted in red. The linker

sequence separating CKB from the FLAG tag is highlighted in grey and the FLAG epitope tag is highlighted in blue. **(c)** Western blot of purified mitochondrial extracts, with and without trypsin treatment, from *Ckb*$^{fl/fl}$ and *Ckb*$^{-/-}$ immortalized brown adipocytes expressing different adenoviral constructs of CKB. **(d)** Creatine kinase (CK) specific activity from protease-treated mitochondrial extracts of *Ckb*$^{fl/fl}$ and *Ckb*$^{-/-}$ immortalized brown adipocytes infected with GFP.FLAG, CKB^{WT}.FLAG, CKB$^{\Delta iMTS\text{-}L}$.FLAG, or CKB^{C283S}.FLAG. Activity was examined in the same protease-treated samples shown in panel (c). Data is expressed as Units/mg protein and was normalized to mitochondrial protein, LONP1. **(e)** Western blot of whole cell extracts or **(f)** post-mitochondrial extracts (also known as the "cytosolic" fraction) from *Ckb*$^{fl/fl}$ and *Ckb*$^{-/-}$ immortalized brown adipocytes infected with GFP.FLAG, CKB^{WT}.FLAG, CKB$^{\Delta iMTS\text{-}L}$.FLAG, or CKB^{C283S}.FLAG. **(g)** Creatine kinase specific activity from post-mitochondrial extracts of *Ckb*$^{fl/fl}$ and *Ckb*$^{-/-}$ immortalized brown adipocytes infected with GFP.FLAG, CKB^{WT}.FLAG, CKB$^{\Delta iMTS\text{-}L}$.FLAG, or CKB^{C283S}.FLAG. Activity was examined in the same protease-treated samples shown in panel (f). **(i)** Western blot of purified mitochondrial extracts, with and without trypsin treatment, from *Ckb*$^{fl/fl}$ and *Ckb*$^{-/-}$ immortalized brown adipocytes infected with *shLacZ* or *shTom70*. Data are expressed as mean ± SEM. of biological replicates. The *p* values shown in figures (d) and (h) were calculated using one-way ANOVA.

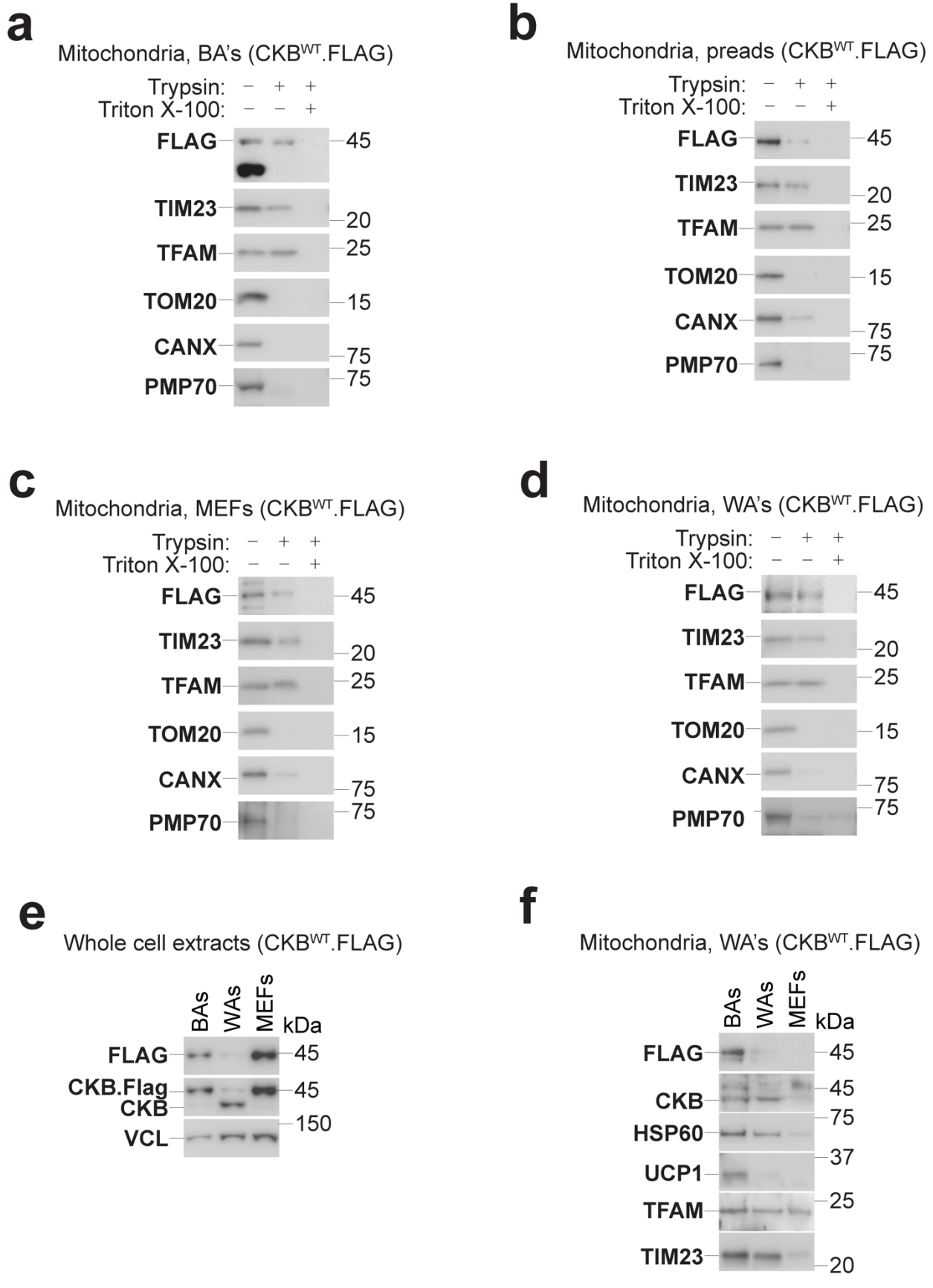
a
Mitochondria, BA's (CKB^WT.FLAG)
Trypsin: − + +
Triton X-100: − − +
FLAG
TIM23
TFAM
TOM20
CANX
PMP70
45
20
25
15
75
75
b
Mitochondria, preads (CKB^WT.FLAG)
Trypsin: − + +
Triton X-100: − − +
FLAG
TIM23
TFAM
TOM20
CANX
PMP70
45
20
25
15
75
75
c
Mitochondria, MEFs (CKB^WT.FLAG)
Trypsin: − + +
Triton X-100: − − +
FLAG
TIM23
TFAM
TOM20
CANX
PMP70
45
20
25
15
75
75
d
Mitochondria, WA's (CKB^WT.FLAG)
Trypsin: − + +
Triton X-100: − − +
FLAG
TIM23
TFAM
TOM20
CANX
PMP70
45
20
25
15
75
75
e
Whole cell extracts (CKB^WT.FLAG)
BAs
WAs
MEFs
kDa
FLAG
CKB.Flag
CKB
VCL
45
45
150
f
Mitochondria, WA's (CKB^WT.FLAG)
BAs
WAs
MEFs
kDa
FLAG
CKB
HSP60
UCP1
TFAM
TIM23
45
45
75
37
25
20

Figure 7. CKB internalization into mitochondria is cell-type dependent

(a) Western blot of mitochondrial extracts, with and without trypsin treatment, purified from primary brown adipocytes (BA's) differentiated *in vitro*, **(b)** primary brown preadipocytes (preads), **(c)** mouse embryonic fibroblasts (MEFs), or **(d)** primary inguinal white adipocytes (WA's) differentiated *in vitroi* expressing CKB^{WT}.FLAG. **(e)** Western blot of whole cell extracts of BA's, WA's, and MEFs expressing CKB^{WT}.FLAG. VCL is a housekeeping protein and was used as a loading control between cell types. **(f)** Western blot of protease-treated mitochondrial extracts from BA's, WA's, and MEFs. Mitochondrial proteins (HSP60, TFAM, TIM23) were used to estimate mitochondrial protein abundance.

VI. DISCUSSION

Futile creatine cycling is a relatively recent mechanism identified in thermogenic adipocytes and the proteins controlling this cycle have yet to be identified. Unpublished data from our lab established that CKB governs PCr generation in brown adipocytes and that loss of *Ckb* leads to blunted rates of oxygen consumption in the same cells. In line with a role as a thermogenic protein, this thesis shows that CKB levels were increased dramatically in murine brown fat following 48 hours and 7 days in the cold compared to brown fat from animals housed at thermoneutrality. Mitochondrial proteins, including components of the ETC, along with GAPDH and VCL were modestly increased by cold exposure, indicating that the increase in CKB was independent of a general increase in protein synthesis. In support of this, the cold-mediated increase in other mitochondrial and cytosolic proteins was only apparent following 7 days in the cold whereas induction of CKB and the canonical thermogenic effector, UCP1, was significant by 48 hours of cold exposure. Surprisingly, *Ckb* mRNA levels were upregulated to a greater degree than *Ucp1*, and Western blotting revealed similar results for CKB protein levels as well. That both CKB protein and mRNA levels are increased after 48 hours in the cold suggests that CKB is regulated at the transcriptional level in response to thermogenic stimuli. Since transcriptional regulation occurs rapidly compared to regulation of protein abundance, examination of *Ckb* mRNA levels in BAT following three hours in the cold could confirm regulation of *Ckb* at the transcript level. The cold-mediated induction of CKB appeared to be selective to BAT, as CKB was not induced in whole tissue lysates from the brain or inguinal white fat of cold-exposed mice compared to mouse housed at thermoneutrality. Given the propensity for beige fat to develop in murine inguinal fat, it is particularly intriguing that CKB was not increased in this adipose depot following cold exposure despite a marked increase in UCP1 levels.

CKB levels were also increased in brown fat of mice treated with CL, a specific β3-adrenergic receptor agonist. Surprisingly, CL appeared to increase BAT CKB levels to a lesser extent than cold, which is surprising given that BAT cold-induced thermogenesis is thought to be mediated exclusively through the β3-adrenergic receptor. These results

suggest that expression of CKB, unlike the canonical thermogenic protein, UCP1, is regulated by a secondary pathway that is activated by cold but independent of β3-adrenergic receptor signaling. One possibility is that full induction of CKB requires synergistic signaling between the β3-adrenergic receptor and some other adrenergic receptor present on brown adipocytes. Since CKB was not induced in inguinal fat of cold-exposed mice, we also hypothesized that if another receptor was regulating CKB levels, it would not be present on the surface of white/beige adipocytes. Mining of independent data revealed that expression of the α1-adrenergic receptor is relatively restricted to the brown fat depot in mice, prompting us to determine the contribution of α1-adrenergic receptor signaling to CKB regulation in murine brown fat.

For *in vivo* studies, mice were treated with the irreversible α-adrenoceptor blocker, phenoxybenzamine, because it is routinely used and exhibits a long half-life (~24 hours). Treating mice with phenoxybenzamine significantly impaired the cold-induced increase in BAT CKB levels, suggesting a role for α-adrenoceptor in regulating CKB levels following sympathetic stimuli. However, phenoxybenzamine was not sufficient to completely override the cold-mediated induction of CKB as BAT CKB levels of cold-exposed mice treated with phenoxybenzamine were still significantly higher compared to mice housed at thermoneutrality. There are two caveats to these observations. First, mice were given phenoxybenzamine by intraperitoneal injection, which leads to systemic distribution of the compound and giving rise to the possibility that inhibition of brown fat CKB induction could be due to off-target effects and not necessarily the result of direct α-adrenoceptor antagonism of BAT. Second, phenoxybenzamine is a non-selective α-adrenoceptor antagonist and blocks all subsets of α-adrenoceptors. However, α2-adrenoceptors are barely expressed on the surface of brown adipocytes and thus, any effects of phenoxybenzamine acting directly on brown fat should only be the result of blocking α1-adrenergic receptor signaling.

In line with *in vivo* observations, *in vitro* studies revealed that brown adipocytes treated with the α1-adrenergic receptor agonist, phenylephrine, exhibited a small, dose-

dependent increase in CKB. However, activation of α-adrenoceptor signaling could not be validated in these studies since known downstream targets of this signaling pathway, such as ERK, were not elevated in brown adipocytes supplemented with phenylephrine. It is possible that ERK phosphorylation induced by α-adrenoceptor signaling is cell type-dependent and that ERK is not a downstream target of the this signaling pathway in primary brown adipocytes differentiated *in vitro*. Since phosphorylation of ERK occurs rapidly following α-adrenoceptor receptor stimulation raises the alternate possibility that the window to measure ERK phosphorylation was missed by the time the cells were harvested. Contrary to *in vivo* experiments, treating primary brown adipocytes with CL or NE was unable to elicit any increase in CKB levels despite strong HSL phosphorylation, indicating activation of β-adrenoceptor signaling. Why stimulation of the β3-adrenergic receptor through treatment with selective (CL) or non-selective (NE) agonists is insufficient to induce CKB levels in brown adipocytes has remained elusive. It is possible that cultured brown adipocytes downregulate a downstream β-adrenoceptor signaling factor that is critical for CKB regulation and is present *in vivo*. Alternatively, it is possible that supplementing brown adipocytes with CL or NE for 24 hours was not long enough to elicit an effect on CKB levels, despite increased lipolytic signaling. *In vitro* supplementation provides a single dose of agonist whereas NE is continually released from sympathetic neurons to activate adrenergic signaling during acute cold exposure in mice. Thus, there are several possibilities why the *in vivo* effects of β3-adrenergic receptor stimulation on CKB levels could not be recapitulated *in vitro*.

The initial data identifying CKB as the creatine kinase isoenzyme controlling creatine cycling in brown adipocyte mitochondria were intriguing given that CKB is typically described of as a “cytosolic” creatine kinase. Indeed, we found that CKB was abundant in cytosolic extracts from brown fat. However, approximately 10% of the total CKB pool was partitioned to mitochondria in BAT from mice housed at room temperature (23°C). Western blotting revealed that abundance of CKB in purified BAT mitochondria increased following 48 hours and 7 days in the cold (6°C), which is similar to observations of whole BAT lysates from the same mice. The mechanism(s) regulating mitochondrial CKB abundance in response to cold exposure are currently unknown. It is possible that

increased CKB levels in mitochondrial extracts from cold-exposed mice is a consequence of increased whole cell CKB levels that occurs in response to cold, and not necessarily a regulatory feature of CKB. Additionally, mitochondrial localization of CKB following cold could be enhanced by post-translational modifications adorned onto CKB following sympathetic stimulation. Several post-translational modifications that affect subcellular protein distribution have been identified and include palmitoylation and glycosylation[171,172].

It was initially hypothesized that there were two distinct isoforms of CKB, a mitochondrial and a cytosolic isoform, and that the mitochondrial isoform was translated from a non-traditional start codon that is present upstream from the canonical M1 start codon of CKB. However, overexpression of the CKB open reading frame was sufficient for mitochondrial targeting in brown adipocytes, nulling this hypothesis. Moreover, overexpression of a CKB variant lacking the first forty amino acids was sufficient for internalization into mitochondria from brown adipocytes, suggesting that the N-termini of CKB did not contain a sequence critical for mitochondrial targeting. In line with this, Western blotting revealed that CKB from mitochondrial and cytosolic extracts showed the same molecular weight. This is an important observation given that most N-terminal MTS are cleaved following stable import of the protein into mitochondria[173,174] and thus, a shorter mitochondrial protein would be expected if CKB import was dependent on an N-terminal MTS. It is perhaps unsurprising that CKB does not contain an N-terminal MTS given that these sequences are mostly found in matrix and inner membrane proteins[174], and that CKB is thought to reside in the IMS. Cysteine motifs are more typical of IMS proteins and are important for IMS protein recognition and import by Mia40[138]. Although cysteine motifs are typically thought to occur as twin CX_3C or CX_9C sequences, recent analysis of the mitochondrial IMS proteome revealed that a number of IMS proteins contain atypical cysteine motifs, including single CX_4C motifs, like that found in CKB[167,168]. Moreover, mitochondrial import of atypical cysteine-containing proteins has been demonstrated to be Mia40-dependent[168]. Thus, it was much more surprising when the $CKB^{C141/6S}$.FLAG variant was readily internalized into brown adipocyte mitochondria.

These data suggest that the CX_4C motif is not important for mitochondrial localization of CKB and thus imply that import of CKB into mitochondria is independent of Mia40.

Closer analysis of the CKB primary sequence revealed that CKB harboured a putative iMTS-L spanning amino acids ~130-10. This was surprising given that iMTS-L are typically found in the carrier family of proteins[175,176]. However, a recent study published in 2018 revealed the presence of iMTS-L in a number of non-mitochondrial annotated proteins that conferred mitochondrial targeting[131]. Since iMTS-L were identified in many non-mitochondrial proteins that were not found in mitochondrial extracts, these authors proposed that the presence of iMTS-L is not necessarily indicative of mitochondrial localization but is also just a general feature of some non-mitochondrial proteins[131]. However, in the case of CKB, mutation of each arginine residue within the putative iMTS-L hindered mitochondrial localization of CKB, suggesting that the iMTS-L allows dual localization of CKB between the cytosol and mitochondria. Canonical iMTS-L-containing carrier proteins have dedicated cytosolic chaperones that ensure efficient mitochondrial translocation of precursor proteins[177], suppressing the possibility of partitioning these proteins to different subcellular compartments. Arginine residues within iMTS-L have been shown to be critical for mitochondrial targeting, and thus were chosen to be replaced with glutamate[178]. Importantly, mutation of the iMTS-L did not disrupt CKB phosphotransferase function or proper protein folding as both CKB^{WT}.FLAG and $CKB^{\Delta iMTS\text{-}L}$.FLAG were able to rescue creatine kinase activity in cytosolic extracts from brown adipocytes expressing each CKB.FLAG variant.

TOM70 is known to recognize carrier proteins harbouring iMTS-L and mediates and/or enhances mitochondrial protein import through direct interaction with critical residues contained within the iMTS-L. Yet, shRNA-mediated reduction of *Tom70* had no effect on the abundance of endogenous CKB in mitochondrial extracts from $Ckb^{fl/fl}$ brown adipocytes. These results do not entirely rule out a role for TOM70 in mitochondrial CKB import. First, mitochondrial proteins tend to have long half-lives compared to other proteins[179], making it is possible that there was simply not enough time between depletion of TOM70 and mitochondrial isolation to see an effect on mitochondrial CKB levels.

Second, it has been reported that import receptors (i.e. TOM70, TOM20, TOM22) share similarities in their substrate spectra and can compensate in the absence of another import receptor[180]. These observations offer another possibility as to why mitochondrial CKB levels are normal in *Tom70*-depleted brown adipocytes. One possible way to probe this would be to subject purified wild-type or *Tom70*$^{-/-}$ brown adipocyte mitochondria to import assays where *Ckb.Flag* is transcribed and translated *in vitro* using rabbit reticulocyte. This approach bypasses adenoviral infection and the possible issue of a long mitochondrial CKB half-life. To address the potential that other import receptors are compensating for the loss of TOM70, *in vitro* import assays will also be performed on mitochondria from brown adipocytes lacking TOM70/TOM20 or TOM70/TOM22. However, it is highly possible that loss of two major mitochondrial import receptors will impact mitochondrial integrity of these cells and may impede this approach.

CKB was also found in mitochondria isolated from murine heart and kidney tissue, although to a much lesser extent compared to CKB levels in mitochondria purified from brown fat. The brain expresses CKB abundantly; however, brain mitochondria were unable to be successfully purified and thus localization of CKB to brain mitochondria was unable to be determined. Why CKB is found at a much higher proportion in brown adipocyte mitochondria is still under investigation. One possibility is simply that brown adipocytes are much more abundant in mitochondria compared to most cell types, leading to greater chances of interactions between CKB and the general mitochondrial import machinery, resulting in enhanced import. A more intriguing possibility is that brown adipocytes possess a unique cytosolic chaperone protein that directs CKB to mitochondria specifically in this cell type.

Similar to brown adipocytes, adenoviral-expressed CKB^{WT}.FLAG was found in protease-treated mitochondrial extracts from primary white adipocytes and MEFs. However, similar to *vivo* results, CKB^{WT}.FLAG was found in brown adipocyte mitochondria at a much higher proportion compared to MEF mitochondria, despite higher CKB^{WT}.FLAG expression in MEF whole cell extracts. Moreover, endogenous levels of CKB were similar between protease-treated mitochondrial extracts from brown and white

adipocytes, despite much higher expression of CKB in primary white adipocyte whole cell extracts. Thus, like other tissue and cell types examined, the proportion of total CKB internalized into white adipocyte mitochondria is much less compared to brown adipocyte mitochondria. Furthermore, adenoviral-expressed CKB^{WT}.FLAG was largely degraded in protease-treated mitochondrial extracts from primary preadipocytes, providing evidence that mitochondrial internalization of CKB is dependent on cell type. Given that the mitochondrial targeting signal is present in the primary sequence of CKB, why CKB is stably imported into mitochondria in some cell types and not others is still unknown. However, our data consistently suggest that mitochondrial import of CKB is enhanced in brown adipocytes both *in vivo* and *in vitro* compared to other tissue and cell types examined. Taken together, these data, along with the observations that CKB is regulated by thermogenic stimuli (i.e. cold), are consistent with a role for CKB in modulating creatine-dependent thermogenesis in brown adipocyte mitochondria. In support of this, unpublished data from our lab demonstrates that creatine is unable to elicit increased respiration in isolated mitochondria from *Ckb*$^{-/-}$ brown adipocytes, whereas creatine robustly stimulates respiration in mitochondria from CKB-expressing cells.

VII. CONCLUSIONS

Adipocyte thermogenesis is leveraged to counteract obesity in mice and brown fat abundance and activity is inversely correlated with BMI in humans, suggesting a protective role against weight gain in both mice and humans. Further understanding of mechanisms driving brown fat thermogenesis are critical to the development of obesity therapeutics. The past five years have seen the identification of new thermogenic pathways that are active in murine brown and beige fat. Unlike UCP1, which stimulates thermogenesis by uncoupling substrate oxidation from ATP synthesis, creatine cycling consumes ATP in a non-productive manner for the cell while simultaneously generating excess ADP that stimulates respiration. Thus, creatine cycling acts as an ATP "sink", which increases substrate flux through the ETC and drives thermogenic respiration. While the basic mechanism by which the creatine cycle operates, and the physiological effects of adipocyte creatine depletion have already been established[96,103,104], the components controlling creatine cycling have not yet been published. The data presented within this thesis stemmed from preliminary observations from our laboratory identifying CKB as the creatine kinase isoenzyme controlling PCr generation for thermogenic creatine cycling. Thus, this first aim of this research was to characterize the thermogenic response of CKB in murine brown fat. Additionally, since CKB is not annotated as a mitochondrial protein, the second aim was to identify the targeting signals that direct CKB to this organelle.

In line with a role in thermogenesis, CKB levels were markedly upregulated in brown fat of cold-exposed mice when compared to mice housed at thermoneutrality. Moreover, signaling through the β3-adrenergic receptor was sufficient to increase CKB levels in thermoneutral-housed animals. Sympathetic activation of adipocyte thermogenesis is thought to be mediated exclusively through the β3-adrenergic receptor. However, inhibition of α-adrenoceptor signaling significantly impaired CKB induction in brown fat of cold-exposed mice, suggesting regulation of CKB by multiple adrenergic pathways. In support of this, activation of α1-adrenergic receptor signaling in primary brown adipocytes augmented CKB levels, although the exact mechanism leading to CKB induction is still under investigation. In addition, CKB levels were unaffected by cold in

murine inguinal white fat, a depot with little to no expression of the α1-adrenergic receptor. Since inguinal WAT abundantly expresses the β3-adrenergic receptor, these observations suggest that synergism between α1-and β3-adrenergic receptor signaling may be required for CKB induction *in vivo*.

Surprisingly, approximately 10% of the total CKB pool is partitioned to mitochondria in brown fat, a much greater proportion (~30X) compared to other CKB-expressing tissues examined (heart and kidney). By analyzing the primary sequence of CKB, different CKB.FLAG variants were generated based on possible mitochondrial targeting sequences identified. Constructs were used for adenoviral expression in primary brown adipocytes and subsequent mitochondrial purification and subjection of organelles to protease treatment as a method of assessing stable import of each CKB.FLAG variant. Using this method, we identify the presence of an iMTS-L in CKB, and that disruption of this sequences leads to $CKB^{\Delta iMTS}$.FLAG degradation in trypsin-treated mitochondrial extracts, indicating impaired mitochondrial import. Overall, these data enhance our molecular understanding of mitochondrial CKB import and lay the framework for studying α-adrenergic receptor regulation of brown fat thermogenesis.

VIII. REFERENCES

1 Organization, W. H. *WHO obesity and overweight fact sheet*, <https://www.who.int/news-room/fact-sheets/detail/obesity-and-overweight> (March 2020).

2 Keys, A., Fidanza, F., Karvonen, M. J., Kimura, N. & Taylor, H. L. Indices of relative weight and obesity. *J Chronic Dis* **25**, 329-343, doi:10.1016/0021-9681(72)90027-6 (1972).

3 Clinical guidelines on the identification, evaluation, and treatment of overweight and obesity in adults: executive summary. Expert Panel on the Identification, Evaluation, and Treatment of Overweight in Adults. *Am J Clin Nutr* **68**, 899-917, doi:10.1093/ajcn/68.4.899 (1998).

4 Romero-Corral, A. *et al.* Accuracy of body mass index in diagnosing obesity in the adult general population. *Int J Obes (Lond)* **32**, 959-966, doi:10.1038/ijo.2008.11 (2008).

5 Flegal, K. M. *et al.* Comparisons of percentage body fat, body mass index, waist circumference, and waist-stature ratio in adults. *Am J Clin Nutr* **89**, 500-508, doi:10.3945/ajcn.2008.26847 (2009).

6 Roche, A. F., Sievogel, R. M., Chumlea, W. C. & Webb, P. Grading body fatness from limited anthropometric data. *Am J Clin Nutr* **34**, 2831-2838, doi:10.1093/ajcn/34.12.2831 (1981).

7 Canada, S. *Overweight and obese adults Health Fact Sheet*, <https://www150.statcan.gc.ca/n1/en/pub/82-625-x/2019001/article/00005-eng.pdf%3Fst%3DOBRuwojR> (June 2019).

8 Heitmann, B. L., Erikson, H., Ellsinger, B. M., Mikkelsen, K. L. & Larsson, B. Mortality associated with body fat, fat-free mass and body mass index among 60-year-old swedish men-a 22-year follow-up. The study of men born in 1913. *Int J Obes Relat Metab Disord* **24**, 33-37, doi:10.1038/sj.ijo.0801082 (2000).

9 Flegal, K. M., Kit, B. K., Orpana, H. & Graubard, B. I. Association of all-cause mortality with overweight and obesity using standard body mass index categories: a systematic review and meta-analysis. *JAMA* **309**, 71-82, doi:10.1001/jama.2012.113905 (2013).

10 Stevens, J. *et al.* Sensitivity and specificity of anthropometrics for the prediction of diabetes in a biracial cohort. *Obes Res* **9**, 696-705, doi:10.1038/oby.2001.94 (2001).

11 Kahn, S. E., Hull, R. L. & Utzschneider, K. M. Mechanisms linking obesity to insulin resistance and type 2 diabetes. *Nature* **444**, 840-846, doi:10.1038/nature05482 (2006).

12 Khan, S. S. *et al.* Association of Body Mass Index With Lifetime Risk of Cardiovascular Disease and Compression of Morbidity. *JAMA Cardiol* **3**, 280-287, doi:10.1001/jamacardio.2018.0022 (2018).

13 Felix-Redondo, F. J. *et al.* Prevalence of obesity and associated cardiovascular risk: the DARIOS study. *BMC Public Health* **13**, 542, doi:10.1186/1471-2458-13-542 (2013).

14 Must, A. *et al.* The disease burden associated with overweight and obesity. *JAMA* **282**, 1523-1529, doi:10.1001/jama.282.16.1523 (1999).

15 Khaodhiar, L., McCowen, K. C. & Blackburn, G. L. Obesity and its comorbid conditions. *Clin Cornerstone* **2**, 17-31, doi:10.1016/s1098-3597(99)90002-9 (1999).

16 Hjartaker, A., Langseth, H. & Weiderpass, E. Obesity and diabetes epidemics: cancer repercussions. *Adv Exp Med Biol* **630**, 72-93, doi:10.1007/978-0-387-78818-0_6 (2008).

17 Janssen, I. The public health burden of obesity in Canada. *Can J Diabetes* **37**, 90-96, doi:10.1016/j.jcjd.2013.02.059 (2013).
18 Ravussin, E. *et al.* Reduced rate of energy expenditure as a risk factor for body-weight gain. *N Engl J Med* **318**, 467-472, doi:10.1056/NEJM198802253180802 (1988).
19 Hill, J. O. & Commerford, R. Physical activity, fat balance, and energy balance. *Int J Sport Nutr* **6**, 80-92, doi:10.1123/ijsn.6.2.80 (1996).
20 Bluher, M. Obesity: global epidemiology and pathogenesis. *Nat Rev Endocrinol* **15**, 288-298, doi:10.1038/s41574-019-0176-8 (2019).
21 Montague, C. T. *et al.* Congenital leptin deficiency is associated with severe early-onset obesity in humans. *Nature* **387**, 903-908, doi:10.1038/43185 (1997).
22 Speliotes, E. K. *et al.* Association analyses of 249,796 individuals reveal 18 new loci associated with body mass index. *Nat Genet* **42**, 937-948, doi:10.1038/ng.686 (2010).
23 Stunkard, A. J., Harris, J. R., Pedersen, N. L. & McClearn, G. E. The body-mass index of twins who have been reared apart. *N Engl J Med* **322**, 1483-1487, doi:10.1056/NEJM199005243222102 (1990).
24 Hopkins, M. *et al.* The adaptive metabolic response to exercise-induced weight loss influences both energy expenditure and energy intake. *Eur J Clin Nutr* **68**, 581-586, doi:10.1038/ejcn.2013.277 (2014).
25 Berthoud, H. R. Homeostatic and non-homeostatic pathways involved in the control of food intake and energy balance. *Obesity (Silver Spring)* **14 Suppl 5**, 197S-200S, doi:10.1038/oby.2006.308 (2006).
26 Hebebrand, J., Volckmar, A. L., Knoll, N. & Hinney, A. Chipping away the 'missing heritability': GIANT steps forward in the molecular elucidation of obesity - but still lots to go. *Obes Facts* **3**, 294-303, doi:10.1159/000321537 (2010).
27 Donnelly, J. E. *et al.* American College of Sports Medicine Position Stand. Appropriate physical activity intervention strategies for weight loss and prevention of weight regain for adults. *Med Sci Sports Exerc* **41**, 459-471, doi:10.1249/MSS.0b013e3181949333 (2009).
28 Mozaffarian, D., Hao, T., Rimm, E. B., Willett, W. C. & Hu, F. B. Changes in diet and lifestyle and long-term weight gain in women and men. *N Engl J Med* **364**, 2392-2404, doi:10.1056/NEJMoa1014296 (2011).
29 Sarlio-Lahteenkorva, S., Rissanen, A. & Kaprio, J. A descriptive study of weight loss maintenance: 6 and 15 year follow-up of initially overweight adults. *Int J Obes Relat Metab Disord* **24**, 116-125, doi:10.1038/sj.ijo.0801094 (2000).
30 Johansson, K., Neovius, K., DeSantis, S. M., Rossner, S. & Neovius, M. Discontinuation due to adverse events in randomized trials of orlistat, sibutramine and rimonabant: a meta-analysis. *Obes Rev* **10**, 564-575, doi:10.1111/j.1467-789X.2009.00581.x (2009).
31 Rothwell, N. J. & Stock, M. J. A role for brown adipose tissue in diet-induced thermogenesis. *Nature* **281**, 31-35, doi:10.1038/281031a0 (1979).
32 Kiess, W. *et al.* Adipocytes and adipose tissue. *Best Pract Res Clin Endocrinol Metab* **22**, 135-153, doi:10.1016/j.beem.2007.10.002 (2008).
33 Xu, H. *et al.* Chronic inflammation in fat plays a crucial role in the development of obesity-related insulin resistance. *J Clin Invest* **112**, 1821-1830, doi:10.1172/JCI19451 (2003).

34 Hotamisligil, G. S., Shargill, N. S. & Spiegelman, B. M. Adipose expression of tumor necrosis factor-alpha: direct role in obesity-linked insulin resistance. *Science* **259**, 87-91, doi:10.1126/science.7678183 (1993).
35 Hirosumi, J. *et al.* A central role for JNK in obesity and insulin resistance. *Nature* **420**, 333-336, doi:10.1038/nature01137 (2002).
36 Yuan, M. *et al.* Reversal of obesity- and diet-induced insulin resistance with salicylates or targeted disruption of Ikkbeta. *Science* **293**, 1673-1677, doi:10.1126/science.1061620 (2001).
37 Cancello, R. *et al.* Increased infiltration of macrophages in omental adipose tissue is associated with marked hepatic lesions in morbid human obesity. *Diabetes* **55**, 1554-1561, doi:10.2337/db06-0133 (2006).
38 Carey, V. J. *et al.* Body fat distribution and risk of non-insulin-dependent diabetes mellitus in women. The Nurses' Health Study. *Am J Epidemiol* **145**, 614-619, doi:10.1093/oxfordjournals.aje.a009158 (1997).
39 Pouliot, M. C. *et al.* Visceral obesity in men. Associations with glucose tolerance, plasma insulin, and lipoprotein levels. *Diabetes* **41**, 826-834, doi:10.2337/diab.41.7.826 (1992).
40 Wang, Y., Rimm, E. B., Stampfer, M. J., Willett, W. C. & Hu, F. B. Comparison of abdominal adiposity and overall obesity in predicting risk of type 2 diabetes among men. *Am J Clin Nutr* **81**, 555-563, doi:10.1093/ajcn/81.3.555 (2005).
41 Kershaw, E. E. & Flier, J. S. Adipose tissue as an endocrine organ. *J Clin Endocrinol Metab* **89**, 2548-2556, doi:10.1210/jc.2004-0395 (2004).
42 Zhang, Y. *et al.* Positional cloning of the mouse obese gene and its human homologue. *Nature* **372**, 425-432, doi:10.1038/372425a0 (1994).
43 Boucher, J. *et al.* Apelin, a newly identified adipokine up-regulated by insulin and obesity. *Endocrinology* **146**, 1764-1771, doi:10.1210/en.2004-1427 (2005).
44 Nicholls, D. G. & Locke, R. M. Thermogenic mechanisms in brown fat. *Physiol Rev* **64**, 1-64, doi:10.1152/physrev.1984.64.1.1 (1984).
45 K., G. Conradi Gesneri medici Tigurine Historiae Animalium: Lib. I De Quadrupedibus viviparis. (1551).
46 Milner, R. E., Wang, L. C. & Trayhurn, P. Brown fat thermogenesis during hibernation and arousal in Richardson's ground squirrel. *Am J Physiol* **256**, R42-48, doi:10.1152/ajpregu.1989.256.1.R42 (1989).
47 Gessner, C., Rondelet, G., Belon, P. & Froschauer, C. *Conradi Gesneri ... Historiae animalium lib. I[-IIII]*. (apvd Christ. Froschoverum, 1551).
48 Foster, D. O. & Frydman, M. L. Nonshivering thermogenesis in the rat. II. Measurements of blood flow with microspheres point to brown adipose tissue as the dominant site of the calorigenesis induced by noradrenaline. *Can J Physiol Pharmacol* **56**, 110-122, doi:10.1139/y78-015 (1978).
49 Foster, D. O. & Frydman, M. L. Tissue distribution of cold-induced thermogenesis in conscious warm- or cold-acclimated rats reevaluated from changes in tissue blood flow: the dominant role of brown adipose tissue in the replacement of shivering by nonshivering thermogenesis. *Can J Physiol Pharmacol* **57**, 257-270, doi:10.1139/y79-039 (1979).
50 Feldmann, H. M., Golozoubova, V., Cannon, B. & Nedergaard, J. UCP1 ablation induces obesity and abolishes diet-induced thermogenesis in mice exempt from thermal stress by

living at thermoneutrality. *Cell Metab* **9**, 203-209, doi:10.1016/j.cmet.2008.12.014 (2009).
51 Kontani, Y. *et al.* UCP1 deficiency increases susceptibility to diet-induced obesity with age. *Aging Cell* **4**, 147-155, doi:10.1111/j.1474-9726.2005.00157.x (2005).
52 van Marken Lichtenbelt, W. D. *et al.* Cold-activated brown adipose tissue in healthy men. *N Engl J Med* **360**, 1500-1508, doi:10.1056/NEJMoa0808718 (2009).
53 Virtanen, K. A. *et al.* Functional brown adipose tissue in healthy adults. *N Engl J Med* **360**, 1518-1525, doi:10.1056/NEJMoa0808949 (2009).
54 Zingaretti, M. C. *et al.* The presence of UCP1 demonstrates that metabolically active adipose tissue in the neck of adult humans truly represents brown adipose tissue. *FASEB J* **23**, 3113-3120, doi:10.1096/fj.09-133546 (2009).
55 Lee, P. *et al.* High prevalence of brown adipose tissue in adult humans. *J Clin Endocrinol Metab* **96**, 2450-2455, doi:10.1210/jc.2011-0487 (2011).
56 Cypess, A. M. *et al.* Identification and importance of brown adipose tissue in adult humans. *N Engl J Med* **360**, 1509-1517, doi:10.1056/NEJMoa0810780 (2009).
57 Ouellet, V. *et al.* Brown adipose tissue oxidative metabolism contributes to energy expenditure during acute cold exposure in humans. *J Clin Invest* **122**, 545-552, doi:10.1172/JCI60433 (2012).
58 van der Lans, A. A. *et al.* Cold acclimation recruits human brown fat and increases nonshivering thermogenesis. *J Clin Invest* **123**, 3395-3403, doi:10.1172/JCI68993 (2013).
59 Vosselman, M. J. *et al.* Brown adipose tissue activity after a high-calorie meal in humans. *Am J Clin Nutr* **98**, 57-64, doi:10.3945/ajcn.113.059022 (2013).
60 M, U. D. *et al.* Postprandial Oxidative Metabolism of Human Brown Fat Indicates Thermogenesis. *Cell Metab* **28**, 207-216 e203, doi:10.1016/j.cmet.2018.05.020 (2018).
61 Yoneshiro, T. *et al.* Brown adipose tissue, whole-body energy expenditure, and thermogenesis in healthy adult men. *Obesity (Silver Spring)* **19**, 13-16, doi:10.1038/oby.2010.105 (2011).
62 Vijgen, G. H. *et al.* Brown adipose tissue in morbidly obese subjects. *PLoS One* **6**, e17247, doi:10.1371/journal.pone.0017247 (2011).
63 Saito, M. *et al.* High incidence of metabolically active brown adipose tissue in healthy adult humans: effects of cold exposure and adiposity. *Diabetes* **58**, 1526-1531, doi:10.2337/db09-0530 (2009).
64 Lee, P., Greenfield, J. R., Ho, K. K. & Fulham, M. J. A critical appraisal of the prevalence and metabolic significance of brown adipose tissue in adult humans. *Am J Physiol Endocrinol Metab* **299**, E601-606, doi:10.1152/ajpendo.00298.2010 (2010).
65 Hossain, M. *et al.* Sinapic acid induces the expression of thermogenic signature genes and lipolysis through activation of PKA/CREB signaling in brown adipocytes. *BMB Rep* **53**, 142-147 (2020).
66 Engel, B. T., Sato, A. & Sato, Y. Responses of sympathetic nerves innervating blood vessels in interscapular, brown adipose tissue and skin during cold stimulation in anesthetized C57BL/6J mice. *Jpn J Physiol* **42**, 549-559, doi:10.2170/jjphysiol.42.549 (1992).
67 Wirsen, C. Adrenergic Innervation of Adipose Tissue Examined by Fluorescence Microscopy. *Nature* **202**, 913, doi:10.1038/202913a0 (1964).

68 Cottle, W. H., Nash, C. W., Veress, A. T. & Ferguson, B. A. Release of noradrenaline from fat of cold-acclimated rats. *Life Sci* **6**, 2267-2271, doi:10.1016/0024-3205(67)90034-3 (1967).
69 Horwitz, B. A., Horowitz, J. M., Jr. & Smith, R. E. Norepinephrine-induced depolarization of brown fat cells. *Proc Natl Acad Sci U S A* **64**, 113-120, doi:10.1073/pnas.64.1.113 (1969).
70 Minneman, K. P., Theroux, T. L., Hollinger, S., Han, C. & Esbenshade, T. A. Selectivity of agonists for cloned alpha 1-adrenergic receptor subtypes. *Mol Pharmacol* **46**, 929-936 (1994).
71 Muzzin, P. *et al.* An adipose tissue-specific beta-adrenergic receptor. Molecular cloning and down-regulation in obesity. *J Biol Chem* **266**, 24053-24058 (1991).
72 Gonzalez, G. A. & Montminy, M. R. Cyclic AMP stimulates somatostatin gene transcription by phosphorylation of CREB at serine 133. *Cell* **59**, 675-680, doi:10.1016/0092-8674(89)90013-5 (1989).
73 Yamamoto, K. K., Gonzalez, G. A., Biggs, W. H., 3rd & Montminy, M. R. Phosphorylation-induced binding and transcriptional efficacy of nuclear factor CREB. *Nature* **334**, 494-498, doi:10.1038/334494a0 (1988).
74 Herzig, S. *et al.* CREB regulates hepatic gluconeogenesis through the coactivator PGC-1. *Nature* **413**, 179-183, doi:10.1038/35093131 (2001).
75 Puigserver, P. *et al.* A cold-inducible coactivator of nuclear receptors linked to adaptive thermogenesis. *Cell* **92**, 829-839, doi:10.1016/s0092-8674(00)81410-5 (1998).
76 Wu, Z. *et al.* Mechanisms controlling mitochondrial biogenesis and respiration through the thermogenic coactivator PGC-1. *Cell* **98**, 115-124, doi:10.1016/S0092-8674(00)80611-X (1999).
77 Rohas, L. M. *et al.* A fundamental system of cellular energy homeostasis regulated by PGC-1alpha. *Proc Natl Acad Sci U S A* **104**, 7933-7938, doi:10.1073/pnas.0702683104 (2007).
78 Couplan, E. *et al.* No evidence for a basal, retinoic, or superoxide-induced uncoupling activity of the uncoupling protein 2 present in spleen or lung mitochondria. *J Biol Chem* **277**, 26268-26275, doi:10.1074/jbc.M202535200 (2002).
79 Nedergaard, J., Bengtsson, T. & Cannon, B. Unexpected evidence for active brown adipose tissue in adult humans. *Am J Physiol Endocrinol Metab* **293**, E444-452, doi:10.1152/ajpendo.00691.2006 (2007).
80 Ricquier, D. & Kader, J. C. Mitochondrial protein alteration in active brown fat: a soidum dodecyl sulfate-polyacrylamide gel electrophoretic study. *Biochem Biophys Res Commun* **73**, 577-583, doi:10.1016/0006-291x(76)90849-4 (1976).
81 Fedorenko, A., Lishko, P. V. & Kirichok, Y. Mechanism of fatty-acid-dependent UCP1 uncoupling in brown fat mitochondria. *Cell* **151**, 400-413, doi:10.1016/j.cell.2012.09.010 (2012).
82 Heaton, G. M., Wagenvoord, R. J., Kemp, A., Jr. & Nicholls, D. G. Brown-adipose-tissue mitochondria: photoaffinity labelling of the regulatory site of energy dissipation. *Eur J Biochem* **82**, 515-521, doi:10.1111/j.1432-1033.1978.tb12045.x (1978).
83 Klingenberg, M. & Winkler, E. The reconstituted isolated uncoupling protein is a membrane potential driven H+ translocator. *EMBO J* **4**, 3087-3092 (1985).

84 Rafael, J. & Heldt, H. W. Binding of guanine nucleotides to the outer surface of the inner membrane of guinea pig brown fat mitochondria in correlation with the thermogenic activity of the tissue. *FEBS Lett* **63**, 304-308, doi:10.1016/0014-5793(76)80117-2 (1976).
85 Rafael, J., Ludolph, H. J. & Hohorst, H. J. [Mitochondria from brown adipose tissue: uncoupling of respiratory chain phosphorylation by long fatty acids and recoupling by guanosine triphosphate]. *Hoppe Seylers Z Physiol Chem* **350**, 1121-1131 (1969).
86 Shabalina, I. G., Jacobsson, A., Cannon, B. & Nedergaard, J. Native UCP1 displays simple competitive kinetics between the regulators purine nucleotides and fatty acids. *J Biol Chem* **279**, 38236-38248, doi:10.1074/jbc.M402375200 (2004).
87 Wu, J. *et al.* Beige adipocytes are a distinct type of thermogenic fat cell in mouse and human. *Cell* **150**, 366-376, doi:10.1016/j.cell.2012.05.016 (2012).
88 Cousin, B. *et al.* Occurrence of brown adipocytes in rat white adipose tissue: molecular and morphological characterization. *J Cell Sci* **103 (Pt 4)**, 931-942 (1992).
89 Himms-Hagen, J. *et al.* Multilocular fat cells in WAT of CL-316243-treated rats derive directly from white adipocytes. *Am J Physiol Cell Physiol* **279**, C670-681, doi:10.1152/ajpcell.2000.279.3.C670 (2000).
90 Golozoubova, V. *et al.* Only UCP1 can mediate adaptive nonshivering thermogenesis in the cold. *FASEB J* **15**, 2048-2050, doi:10.1096/fj.00-0536fje (2001).
91 Hofmann, W. E., Liu, X., Bearden, C. M., Harper, M. E. & Kozak, L. P. Effects of genetic background on thermoregulation and fatty acid-induced uncoupling of mitochondria in UCP1-deficient mice. *J Biol Chem* **276**, 12460-12465, doi:10.1074/jbc.M100466200 (2001).
92 Liu, X. *et al.* Paradoxical resistance to diet-induced obesity in UCP1-deficient mice. *J Clin Invest* **111**, 399-407, doi:10.1172/JCI15737 (2003).
93 Lowell, B. B. *et al.* Development of obesity in transgenic mice after genetic ablation of brown adipose tissue. *Nature* **366**, 740-742, doi:10.1038/366740a0 (1993).
94 Enerback, S. *et al.* Mice lacking mitochondrial uncoupling protein are cold-sensitive but not obese. *Nature* **387**, 90-94, doi:10.1038/387090a0 (1997).
95 Ikeda, K. *et al.* UCP1-independent signaling involving SERCA2b-mediated calcium cycling regulates beige fat thermogenesis and systemic glucose homeostasis. *Nat Med* **23**, 1454-1465, doi:10.1038/nm.4429 (2017).
96 Kazak, L. *et al.* A creatine-driven substrate cycle enhances energy expenditure and thermogenesis in beige fat. *Cell* **163**, 643-655, doi:10.1016/j.cell.2015.09.035 (2015).
97 Bessman, S. P. & Geiger, P. J. Transport of energy in muscle: the phosphorylcreatine shuttle. *Science* **211**, 448-452, doi:10.1126/science.6450446 (1981).
98 Jacobus, W. E. & Lehninger, A. L. Creatine kinase of rat heart mitochondria. Coupling of creatine phosphorylation to electron transport. *J Biol Chem* **248**, 4803-4810 (1973).
99 Wallimann, T., Wyss, M., Brdiczka, D., Nicolay, K. & Eppenberger, H. M. Intracellular compartmentation, structure and function of creatine kinase isoenzymes in tissues with high and fluctuating energy demands: the 'phosphocreatine circuit' for cellular energy homeostasis. *Biochem J* **281 (Pt 1)**, 21-40, doi:10.1042/bj2810021 (1992).
100 Haas, R. C. & Strauss, A. W. Separate nuclear genes encode sarcomere-specific and ubiquitous human mitochondrial creatine kinase isoenzymes. *J Biol Chem* **265**, 6921-6927 (1990).

101 Hossle, J. P. *et al.* Distinct tissue specific mitochondrial creatine kinases from chicken brain and striated muscle with a conserved CK framework. *Biochem Biophys Res Commun* **151**, 408-416, doi:10.1016/0006-291x(88)90608-0 (1988).
102 Roesler, A. & Kazak, L. UCP1-independent thermogenesis. *Biochem J* **477**, 709-725, doi:10.1042/BCJ20190463 (2020).
103 Kazak, L. *et al.* Genetic Depletion of Adipocyte Creatine Metabolism Inhibits Diet-Induced Thermogenesis and Drives Obesity. *Cell Metab* **26**, 693, doi:10.1016/j.cmet.2017.09.007 (2017).
104 Kazak, L. *et al.* Ablation of adipocyte creatine transport impairs thermogenesis and causes diet-induced obesity. *Nat Metab* **1**, 360-370, doi:10.1038/s42255-019-0035-x (2019).
105 Rath, S. *et al.* MitoCarta3.0: an updated mitochondrial proteome now with sub-organelle localization and pathway annotations. *Nucleic Acids Res*, doi:10.1093/nar/gkaa1011 (2020).
106 Anderson, S. *et al.* Sequence and organization of the human mitochondrial genome. *Nature* **290**, 457-465, doi:10.1038/290457a0 (1981).
107 Pagliarini, D. J. *et al.* A mitochondrial protein compendium elucidates complex I disease biology. *Cell* **134**, 112-123, doi:10.1016/j.cell.2008.06.016 (2008).
108 Chacinska, A., Koehler, C. M., Milenkovic, D., Lithgow, T. & Pfanner, N. Importing mitochondrial proteins: machineries and mechanisms. *Cell* **138**, 628-644, doi:10.1016/j.cell.2009.08.005 (2009).
109 Hill, K. *et al.* Tom40 forms the hydrophilic channel of the mitochondrial import pore for preproteins [see comment]. *Nature* **395**, 516-521, doi:10.1038/26780 (1998).
110 Kiebler, M. *et al.* Identification of a mitochondrial receptor complex required for recognition and membrane insertion of precursor proteins. *Nature* **348**, 610-616, doi:10.1038/348610a0 (1990).
111 Shiota, T. *et al.* Molecular architecture of the active mitochondrial protein gate. *Science* **349**, 1544-1548, doi:10.1126/science.aac6428 (2015).
112 Abe, Y. *et al.* Structural basis of presequence recognition by the mitochondrial protein import receptor Tom20. *Cell* **100**, 551-560, doi:10.1016/s0092-8674(00)80691-1 (2000).
113 Hurt, E. C., Pesold-Hurt, B. & Schatz, G. The cleavable prepiece of an imported mitochondrial protein is sufficient to direct cytosolic dihydrofolate reductase into the mitochondrial matrix. *FEBS Lett* **178**, 306-310, doi:10.1016/0014-5793(84)80622-5 (1984).
114 Roise, D., Horvath, S. J., Tomich, J. M., Richards, J. H. & Schatz, G. A chemically synthesized pre-sequence of an imported mitochondrial protein can form an amphiphilic helix and perturb natural and artificial phospholipid bilayers. *EMBO J* **5**, 1327-1334 (1986).
115 Bolliger, L., Junne, T., Schatz, G. & Lithgow, T. Acidic receptor domains on both sides of the outer membrane mediate translocation of precursor proteins into yeast mitochondria. *EMBO J* **14**, 6318-6326 (1995).
116 Moczko, M. *et al.* The intermembrane space domain of mitochondrial Tom22 functions as a trans binding site for preproteins with N-terminal targeting sequences. *Mol Cell Biol* **17**, 6574-6584, doi:10.1128/mcb.17.11.6574 (1997).

117 Chacinska, A. *et al.* Mitochondrial presequence translocase: switching between TOM tethering and motor recruitment involves Tim21 and Tim17. *Cell* **120**, 817-829, doi:10.1016/j.cell.2005.01.011 (2005).
118 Mokranjac, D. *et al.* Role of Tim50 in the transfer of precursor proteins from the outer to the inner membrane of mitochondria. *Mol Biol Cell* **20**, 1400-1407, doi:10.1091/mbc.E08-09-0934 (2009).
119 van der Laan, M. *et al.* Motor-free mitochondrial presequence translocase drives membrane integration of preproteins. *Nat Cell Biol* **9**, 1152-1159, doi:10.1038/ncb1635 (2007).
120 Martin, J., Mahlke, K. & Pfanner, N. Role of an energized inner membrane in mitochondrial protein import. Delta psi drives the movement of presequences. *J Biol Chem* **266**, 18051-18057 (1991).
121 Turakhiya, U. *et al.* Protein Import by the Mitochondrial Presequence Translocase in the Absence of a Membrane Potential. *J Mol Biol* **428**, 1041-1052, doi:10.1016/j.jmb.2016.01.020 (2016).
122 Horst, M. *et al.* Sequential action of two hsp70 complexes during protein import into mitochondria. *EMBO J* **16**, 1842-1849, doi:10.1093/emboj/16.8.1842 (1997).
123 Kang, P. J. *et al.* Requirement for hsp70 in the mitochondrial matrix for translocation and folding of precursor proteins. *Nature* **348**, 137-143, doi:10.1038/348137a0 (1990).
124 Cyr, D. M., Stuart, R. A. & Neupert, W. A matrix ATP requirement for presequence translocation across the inner membrane of mitochondria. *J Biol Chem* **268**, 23751-23754 (1993).
125 Hawlitschek, G. *et al.* Mitochondrial protein import: identification of processing peptidase and of PEP, a processing enhancing protein. *Cell* **53**, 795-806, doi:10.1016/0092-8674(88)90096-7 (1988).
126 Hell, K., Neupert, W. & Stuart, R. A. Oxa1p acts as a general membrane insertion machinery for proteins encoded by mitochondrial DNA. *EMBO J* **20**, 1281-1288, doi:10.1093/emboj/20.6.1281 (2001).
127 Rojo, E. E., Stuart, R. A. & Neupert, W. Conservative sorting of F0-ATPase subunit 9: export from matrix requires delta pH across inner membrane and matrix ATP. *EMBO J* **14**, 3445-3451 (1995).
128 Hartl, F. U., Schmidt, B., Wachter, E., Weiss, H. & Neupert, W. Transport into mitochondria and intramitochondrial sorting of the Fe/S protein of ubiquinol-cytochrome c reductase. *Cell* **47**, 939-951, doi:10.1016/0092-8674(86)90809-3 (1986).
129 Stiller, S. B. *et al.* Mitochondrial OXA Translocase Plays a Major Role in Biogenesis of Inner-Membrane Proteins. *Cell Metab* **23**, 901-908, doi:10.1016/j.cmet.2016.04.005 (2016).
130 Brix, J., Rudiger, S., Bukau, B., Schneider-Mergener, J. & Pfanner, N. Distribution of binding sequences for the mitochondrial import receptors Tom20, Tom22, and Tom70 in a presequence-carrying preprotein and a non-cleavable preprotein. *J Biol Chem* **274**, 16522-16530, doi:10.1074/jbc.274.23.16522 (1999).
131 Backes, S. *et al.* Tom70 enhances mitochondrial preprotein import efficiency by binding to internal targeting sequences. *J Cell Biol* **217**, 1369-1382, doi:10.1083/jcb.201708044 (2018).
132 Bihlmaier, K. *et al.* The disulfide relay system of mitochondria is connected to the respiratory chain. *J Cell Biol* **179**, 389-395, doi:10.1083/jcb.200707123 (2007).

133 Mesecke, N. *et al.* A disulfide relay system in the intermembrane space of mitochondria that mediates protein import. *Cell* **121**, 1059-1069, doi:10.1016/j.cell.2005.04.011 (2005).
134 Chacinska, A. *et al.* Essential role of Mia40 in import and assembly of mitochondrial intermembrane space proteins. *EMBO J* **23**, 3735-3746, doi:10.1038/sj.emboj.7600389 (2004).
135 Naoe, M. *et al.* Identification of Tim40 that mediates protein sorting to the mitochondrial intermembrane space. *J Biol Chem* **279**, 47815-47821, doi:10.1074/jbc.M410272200 (2004).
136 Terziyska, N. *et al.* Mia40, a novel factor for protein import into the intermembrane space of mitochondria is able to bind metal ions. *FEBS Lett* **579**, 179-184, doi:10.1016/j.febslet.2004.11.072 (2005).
137 Lee, J., Hofhaus, G. & Lisowsky, T. Erv1p from Saccharomyces cerevisiae is a FAD-linked sulfhydryl oxidase. *FEBS Lett* **477**, 62-66, doi:10.1016/s0014-5793(00)01767-1 (2000).
138 Allen, S., Balabanidou, V., Sideris, D. P., Lisowsky, T. & Tokatlidis, K. Erv1 mediates the Mia40-dependent protein import pathway and provides a functional link to the respiratory chain by shuttling electrons to cytochrome c. *J Mol Biol* **353**, 937-944, doi:10.1016/j.jmb.2005.08.049 (2005).
139 Jores, T. *et al.* Characterization of the targeting signal in mitochondrial beta-barrel proteins. *Nat Commun* **7**, 12036, doi:10.1038/ncomms12036 (2016).
140 Paschen, S. A. *et al.* Evolutionary conservation of biogenesis of beta-barrel membrane proteins. *Nature* **426**, 862-866, doi:10.1038/nature02208 (2003).
141 Wiedemann, N. *et al.* Machinery for protein sorting and assembly in the mitochondrial outer membrane. *Nature* **424**, 565-571, doi:10.1038/nature01753 (2003).
142 Walther, D. M., Papic, D., Bos, M. P., Tommassen, J. & Rapaport, D. Signals in bacterial beta-barrel proteins are functional in eukaryotic cells for targeting to and assembly in mitochondria. *Proc Natl Acad Sci U S A* **106**, 2531-2536, doi:10.1073/pnas.0807830106 (2009).
143 Dukanovic, J. & Rapaport, D. Multiple pathways in the integration of proteins into the mitochondrial outer membrane. *Biochim Biophys Acta* **1808**, 971-980, doi:10.1016/j.bbamem.2010.06.021 (2011).
144 Becker, T. *et al.* Biogenesis of the mitochondrial TOM complex: Mim1 promotes insertion and assembly of signal-anchored receptors. *J Biol Chem* **283**, 120-127, doi:10.1074/jbc.M706997200 (2008).
145 Popov-Celeketic, J., Waizenegger, T. & Rapaport, D. Mim1 functions in an oligomeric form to facilitate the integration of Tom20 into the mitochondrial outer membrane. *J Mol Biol* **376**, 671-680, doi:10.1016/j.jmb.2007.12.006 (2008).
146 Hulett, J. M. *et al.* The transmembrane segment of Tom20 is recognized by Mim1 for docking to the mitochondrial TOM complex. *J Mol Biol* **376**, 694-704, doi:10.1016/j.jmb.2007.12.021 (2008).
147 Setoguchi, K., Otera, H. & Mihara, K. Cytosolic factor- and TOM-independent import of C-tail-anchored mitochondrial outer membrane proteins. *EMBO J* **25**, 5635-5647, doi:10.1038/sj.emboj.7601438 (2006).

148 Krumpe, K. *et al.* Ergosterol content specifies targeting of tail-anchored proteins to mitochondrial outer membranes. *Mol Biol Cell* **23**, 3927-3935, doi:10.1091/mbc.E11-12-0994 (2012).
149 Kemper, C. *et al.* Integration of tail-anchored proteins into the mitochondrial outer membrane does not require any known import components. *J Cell Sci* **121**, 1990-1998, doi:10.1242/jcs.024034 (2008).
150 Schmidt, O. *et al.* Regulation of mitochondrial protein import by cytosolic kinases. *Cell* **144**, 227-239, doi:10.1016/j.cell.2010.12.015 (2011).
151 Boos, F., Mühlhaus, T. and Herrmann, J. M. . Detection of Internal Matrix Targeting Signal-like Sequences (iMTS-Ls) in Mitochondrial Precursor Proteins Using the TargetP Prediction Tool. *Bio-protocol* **8**, e2474, doi:10.21769/BioProtoc.2474 (2018).
152 Emanuelsson, O., Brunak, S., von Heijne, G. & Nielsen, H. Locating proteins in the cell using TargetP, SignalP and related tools. *Nat Protoc* **2**, 953-971, doi:10.1038/nprot.2007.131 (2007).
153 Okamatsu-Ogura, Y. *et al.* Thermogenic ability of uncoupling protein 1 in beige adipocytes in mice. *PLoS One* **8**, e84229, doi:10.1371/journal.pone.0084229 (2013).
154 Shabalina, I. G. *et al.* UCP1 in brite/beige adipose tissue mitochondria is functionally thermogenic. *Cell Rep* **5**, 1196-1203, doi:10.1016/j.celrep.2013.10.044 (2013).
155 Collins, S., Daniel, K. W., Petro, A. E. & Surwit, R. S. Strain-specific response to beta 3-adrenergic receptor agonist treatment of diet-induced obesity in mice. *Endocrinology* **138**, 405-413, doi:10.1210/endo.138.1.4829 (1997).
156 Ferrannini, G. *et al.* Genetic backgrounds determine brown remodeling of white fat in rodents. *Mol Metab* **5**, 948-958, doi:10.1016/j.molmet.2016.08.013 (2016).
157 Cannon, B. & Nedergaard, J. Brown adipose tissue: function and physiological significance. *Physiol Rev* **84**, 277-359, doi:10.1152/physrev.00015.2003 (2004).
158 Susulic, V. S. *et al.* Targeted disruption of the beta 3-adrenergic receptor gene. *J Biol Chem* **270**, 29483-29492, doi:10.1074/jbc.270.49.29483 (1995).
159 Zhao, J., Unelius, L., Bengtsson, T., Cannon, B. & Nedergaard, J. Coexisting beta-adrenoceptor subtypes: significance for thermogenic process in brown fat cells. *Am J Physiol* **267**, C969-979, doi:10.1152/ajpcell.1994.267.4.C969 (1994).
160 Mohell, N., Nedergaard, J. & Cannon, B. Quantitative differentiation of alpha- and beta-adrenergic respiratory responses in isolated hamster brown fat cells: evidence for the presence of an alpha 1-adrenergic component. *Eur J Pharmacol* **93**, 183-193, doi:10.1016/0014-2999(83)90136-x (1983).
161 Zhao, J., Cannon, B. & Nedergaard, J. alpha1-Adrenergic stimulation potentiates the thermogenic action of beta3-adrenoreceptor-generated cAMP in brown fat cells. *J Biol Chem* **272**, 32847-32856, doi:10.1074/jbc.272.52.32847 (1997).
162 Beak, J. *et al.* An Oral Selective Alpha-1A Adrenergic Receptor Agonist Prevents Doxorubicin Cardiotoxicity. *JACC Basic Transl Sci* **2**, 39-53, doi:10.1016/j.jacbts.2016.10.006 (2017).
163 Fulghum, K. L. *et al.* Mitochondria-associated lactate dehydrogenase is not a biologically significant contributor to bioenergetic function in murine striated muscle. *Redox Biol* **24**, 101177, doi:10.1016/j.redox.2019.101177 (2019).
164 Ieva, R. *et al.* Mitochondrial inner membrane protease promotes assembly of presequence translocase by removing a carboxy-terminal targeting sequence. *Nat Commun* **4**, 2853, doi:10.1038/ncomms3853 (2013).

165 Kazak, L. *et al.* Alternative translation initiation augments the human mitochondrial proteome. *Nucleic Acids Res* **41**, 2354-2369, doi:10.1093/nar/gks1347 (2013).
166 Silvestri, L. *et al.* Mitochondrial import and enzymatic activity of PINK1 mutants associated to recessive parkinsonism. *Hum Mol Genet* **14**, 3477-3492, doi:10.1093/hmg/ddi377 (2005).
167 Nuebel, E., Manganas, P. & Tokatlidis, K. Orphan proteins of unknown function in the mitochondrial intermembrane space proteome: New pathways and metabolic cross-talk. *Biochim Biophys Acta* **1863**, 2613-2623, doi:10.1016/j.bbamcr.2016.07.004 (2016).
168 Vogtle, F. N. *et al.* Intermembrane space proteome of yeast mitochondria. *Mol Cell Proteomics* **11**, 1840-1852, doi:10.1074/mcp.M112.021105 (2012).
169 Woellhaf, M. W., Sommer, F., Schroda, M. & Herrmann, J. M. Proteomic profiling of the mitochondrial ribosome identifies Atp25 as a composite mitochondrial precursor protein. *Mol Biol Cell* **27**, 3031-3039, doi:10.1091/mbc.E16-07-0513 (2016).
170 Long, J. Z. *et al.* A smooth muscle-like origin for beige adipocytes. *Cell Metab* **19**, 810-820, doi:10.1016/j.cmet.2014.03.025 (2014).
171 Druey, K. M. *et al.* Amino-terminal cysteine residues of RGS16 are required for palmitoylation and modulation of Gi- and Gq-mediated signaling. *J Biol Chem* **274**, 18836-18842, doi:10.1074/jbc.274.26.18836 (1999).
172 Rakus, J. F. & Mahal, L. K. New technologies for glycomic analysis: toward a systematic understanding of the glycome. *Annu Rev Anal Chem (Palo Alto Calif)* **4**, 367-392, doi:10.1146/annurev-anchem-061010-113951 (2011).
173 Taylor, A. B. *et al.* Crystal structures of mitochondrial processing peptidase reveal the mode for specific cleavage of import signal sequences. *Structure* **9**, 615-625, doi:10.1016/s0969-2126(01)00621-9 (2001).
174 Vogtle, F. N. *et al.* Global analysis of the mitochondrial N-proteome identifies a processing peptidase critical for protein stability. *Cell* **139**, 428-439, doi:10.1016/j.cell.2009.07.045 (2009).
175 Pfanner, N., Hoeben, P., Tropschug, M. & Neupert, W. The carboxyl-terminal two-thirds of the ADP/ATP carrier polypeptide contains sufficient information to direct translocation into mitochondria. *J Biol Chem* **262**, 14851-14854 (1987).
176 Sirrenberg, C. *et al.* Carrier protein import into mitochondria mediated by the intermembrane proteins Tim10/Mrs11 and Tim12/Mrs5. *Nature* **391**, 912-915, doi:10.1038/36136 (1998).
177 Young, J. C., Hoogenraad, N. J. & Hartl, F. U. Molecular chaperones Hsp90 and Hsp70 deliver preproteins to the mitochondrial import receptor Tom70. *Cell* **112**, 41-50, doi:10.1016/s0092-8674(02)01250-3 (2003).
178 Suzuki, H., Maeda, M. & Mihara, K. Characterization of rat TOM70 as a receptor of the preprotein translocase of the mitochondrial outer membrane. *J Cell Sci* **115**, 1895-1905 (2002).
179 Price, J. C., Guan, S., Burlingame, A., Prusiner, S. B. & Ghaemmaghami, S. Analysis of proteome dynamics in the mouse brain. *Proc Natl Acad Sci U S A* **107**, 14508-14513, doi:10.1073/pnas.1006551107 (2010).
180 Ramage, L., Junne, T., Hahne, K., Lithgow, T. & Schatz, G. Functional cooperation of mitochondrial protein import receptors in yeast. *EMBO J* **12**, 4115-4123 (1993).